INFORMATION TO USERS

This manuscript has been reproduced from the microfilm master. UMI films the text directly from the original or copy submitted. Thus, some thesis and dissertation copies are in typewriter face, while others may be from any type of computer printer.

The quality of this reproduction is dependent upon the quality of the copy submitted. Broken or indistinct print, colored or poor quality illustrations and photographs, print bleedthrough, substandard margins, and improper alignment can adversely affect reproduction.

In the unlikely event that the author did not send UMI a complete manuscript and there are missing pages, these will be noted. Also, if unauthorized copyright material had to be removed, a note will indicate the deletion.

Oversize materials (e.g., maps, drawings, charts) are reproduced by sectioning the original, beginning at the upper left-hand corner and continuing from left to right in equal sections with small overlaps. Each original is also photographed in one exposure and is included in reduced form at the back of the book.

Photographs included in the original manuscript have been reproduced xerographically in this copy. Higher quality 6" x 9" black and white photographic prints are available for any photographs or illustrations appearing in this copy for an additional charge. Contact UMI directly to order.

UMI®

Bell & Howell Information and Learning
300 North Zeeb Road, Ann Arbor, MI 48106-1346 USA
800-521-0600

A Continuous Spectrophotometric Assay for Phosphate Releasing Enzymes.

Colin E. Rieger

A thesis

in

The Department

of

Chemistry and Biochemistry

Presented in Partial Fulfilment of the Requirements
for the Degree of Master of Science at
Concordia University
Montreal, Quebec, Canada

April 1998

ABSTRACT

A Continuous Spectrophotometric Assay
for Phosphate Releasing Enzymes.

Colin E. Rieger

A new continuous coupled UV-spectrophotometric assay is described for two phosphate releasing enzymes, aspartate transcarbamylase and ATPase of Herpes Simplex Virus. Phosphate release is coupled to the phosphorolysis of the nucleoside analogue 7-methylinosine catalyzed by purine nucleoside phosphorylase. When this reaction is monitored at 291 nm, the coupled assay can readily detect 10 nmol P_i released/min. Our method offers advantages over a recently reported continuous assay devised for measuring ATCase activity using the nucleoside analogue methylthioguanosine as the linking substrate. In contrast to MESG, m^7Ino is easily and inexpensively synthesized and is also commercially available. The spectrophotometric signal at 291 nm, produced by the difference in the extinction coefficients between nucleoside substrate and the base product, is significant over a much wider pH range than the signal difference between MESG and its phosphorolysis product at 360 nm. Saturation curves for aspartate and carbamyl phosphate and pH rate profiles have been reproduced using the PNPase/m^7Ino coupled assay. Initial velocity patterns constructed over micromolar to millimolar concentrations of aspartate and CbmP yield four kinetic parameters simultaneously. To further illustrate the application of this coupled assay, kinetic parameters were determined for the DNA-dependent ATPase reaction of HSV helicase-primase.

ACKNOWLEDGMENTS

I am grateful to Bio-Mega/Boehringer Ingleheim Research, Inc. (Quebec) for their gift of HSV-1 helicase-primase. I thank Glenn Stanisforth, and Ying Yang for providing the impetus to initiate this work, Dr. Peter White for helpful discussions, and John Lee for his work in providing (practically) unlimited quantities of PNPase. I would like to thank Dinesh Christiandat for his entertaining and stimulating lab-companionship during my stay in Montreal. Lastly and mostly I would like to thank my supervisor, Dr. Joanne Turnbull, for allowing me to pursue this work, and providing help in too many ways to mention. This thesis, and the paper it became, would be much less without the kinetic knowledge and experience Joanne provided. This research was funded by a Concordia University Faculty Development Award and by the Natural Sciences and Engineering Research Council of Canada.

TABLE OF CONTENTS

LIST OF FIGURES

LIST OF FIGURES (CONT.)

LIST OF FIGURES (CONT.)

Page

LIST OF FIGURES (CONT.)

LIST OF TABLES AND ABBREVIATIONS

Abbreviations used: ATCase, aspartate transcarbamylase; CbmP, carbamyl phosphate; HSV, herpes simplex virus; m^7Guo, 7-methylguanosine; m^7Hx, 7-methylhypoxanthine; m^7Ino, 7-methylinosine; MES, 2-(N-morpholino)ethanesulfonic acid; MESG, 7-methyl-6-thioguanosine; MOPS, 3-(N-morpholino)propanesulfonic acid.

1. INTRODUCTION

1.1 The Development of a Continuous Phosphate Assay

Kinetic studies of phosphate liberating enzymes have, in the past, generally relied upon the use of stop-time radioactive or colorimetric assays. Radioactive assays have taken many forms, but stop-time colorimetric phosphate assays often utilize molybdenum salts (1). Such assays are, however, cumbersome and laborious and are an unsatisfactory solution for the assay of phosphate liberating enzymes.

Until recently, no continuous assay for the detection of free phosphate has been developed that is sensitive yet also convenient and cost effective. Figure 1 shows several linked, continuous phosphate assays. The glycogen phosphorylase assay to continuously monitor the liberation of phosphate requires two coupling substrates and three coupling enzymes, and spectrophotometrically monitors the reduction of $NADP^+$ (2). The xanthine oxidase-coupled phosphate assay monitors the production of uric acid at 302 nm and requires the addition of two enzymes and one substrate (3).

A) The glycogen phosphorylase assay

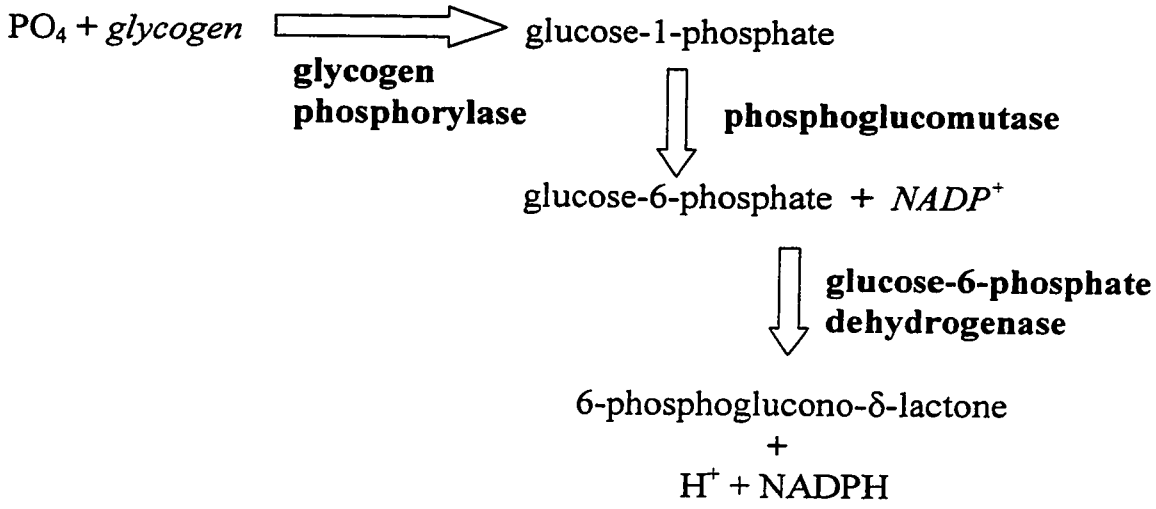

B) The xanthine oxidase-coupled phosphate assay

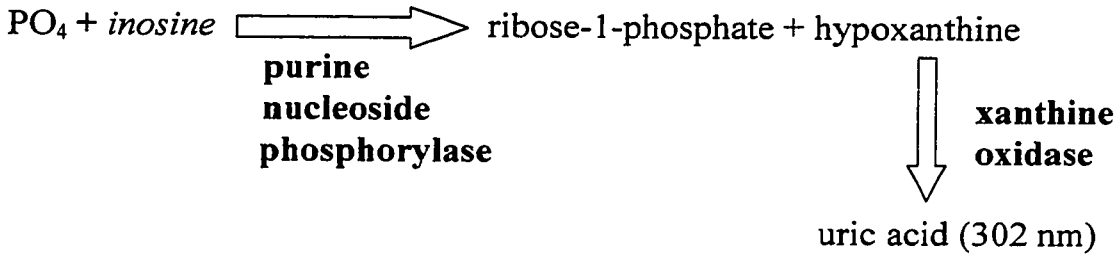

C) The Purine Nucleoside Phosphorylase Assay

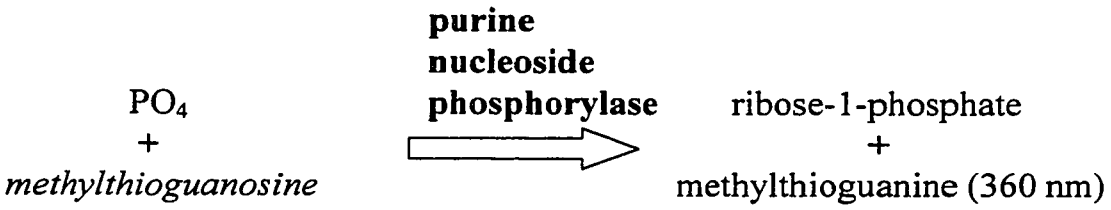

Figure 1: Some linked spectrophotometric assays for phosphate liberating enzymes. Required linking reagents are shown in bold (**enzymes**) and italics (*substrates*).

Factors which must be closely considered when using multiply-coupled systems such as the xanthine oxidase and glycogen phosphorylase assays include cost, lag times, the introduction of rate limiting steps, ionic and other non-specific effects. These continuous assays are thus useful under a limited range of conditions. A truly useful continuous assay would have one linking enzyme and one linking substrate, both of which are easily obtainable and cost efficient. As spectrophotometers are generally available to most researchers, another requirement for a continuous phosphate assay would be for a spectrophotometric signal.

Recently, purine nucleoside phosphorylase (PNPase (**3**), EC 2.4.2.1), has been used in a continuous phosphate assay that uses only one enzyme and one substrate (Figure 1). PNPase is an enzyme in the purine salvage pathway of both eukaryotes and prokaryotes (**4**). Bacterial PNPase catalyzes the reversible phosphorolysis of adenine, hypoxanthine, or guanine (deoxy)ribonucleosides yielding the purine base and (deoxy)ribose 1-phosphate (Figure 2) (**5**). This lack of substrate specificity initially generated interest in PNPase as a tool in synthetic organic chemistry by allowing the assembly of synthetic purine nucleosides from substituted purine bases and (deoxy)ribose 1-phosphate (**6**). However, the spectral characteristics of some of the synthetic substrates soon led to the development of both fluorescent and spectrophotometric PNPase-coupled phosphate assays.

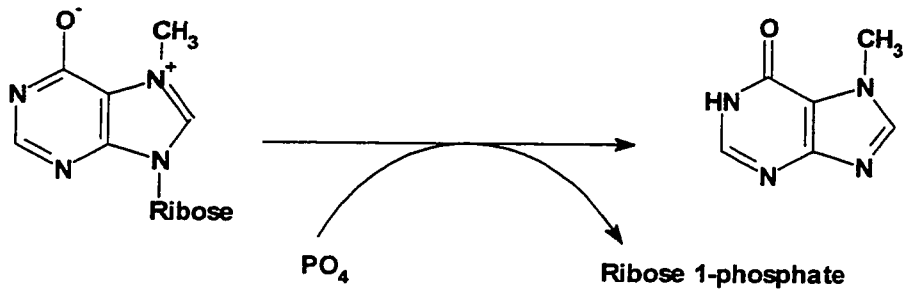

Figure 2: The phosphorolysis of m^7Ino catalyzed by PNPase

Both 7-methylinosine (m^7Ino) and 7-methylguanosine (m^7Guo) are good substrates of PNPase and exhibit both fluorescence and absorbance changes upon phosphorolysis (**7**). The combination of m^7Guo and PNPase has been used in coupled fluorescent assays of enzymes exhibiting ATPase activity (**8**, **9**). The absorbance properties of either of these two purine nucleosides have not yet been exploited in a coupled assay.

Another synthetic substrate, 7-methyl-6-thioguanosine (MESG), has been used in a continuous spectrophotometric phosphate assay to monitor the activities of several ATPases (**10**), aspartate transcarbamylase (**11**), protein phosphatases (**12**), and pyrophosphate releasing enzymes (**13**). Despite the apparent utility of the PNPase/MESG coupled spectrophotometric assay, MESG itself is not commercially available and is both laborious and expensive to synthesize (**14**). Further, MESG is insoluble at greater than low mM concentrations, and the spectrophotometric signal at 360 nm is limited to a pH range of about 6.5 - 8.8 (**8**, **10**). It is the ionization states of the nucleoside substrates and their respective products at a given pH, and the extinction coefficient for each species, that determines the maximum obtainable signal (**7**, **10**). A kit form of the MESG/PNPase assay is now available but some researchers have raised concern as to the purity of the commercially provided PNPase.

This work demonstrates that m^7Ino has suitable spectral characteristics that allow its use as a linking substrate for a continuous UV-spectrophotometric assay for phosphate-releasing enzymes over a wide pH range. m^7Ino has a maximum absorbance at 265 nm but it shows a significant change in absorbance from its phosphorolysis product, 7-methylhypoxanthine (m^7Hx) between 280 - 290 nm at neutral pH (7).

The potential of the PNPase/m^7Ino coupled phosphate assay is illustrated through the kinetic studies of two phosphate-releasing enzymes, aspartate transcarbamylase (ATCase), and the ATPase activity from the Herpes Simplex Virus type 1 (HSV-1) helicase-primase enzyme.

1.2 Introduction to Aspartate Transcarbamlyase

1.2.1 General Introduction to ATCase

ATCase catalyses the initial committed step of the pyrimidine biosynthesis pathway in all organisms:

L-aspartate + carbamyl phosphate → N-carbamyl-L-aspartate + P_i

Due to its importance in nucleotide synthesis, ATCase has been a target for antineoplastic, antiparasitic, and antimicrobial agents (**15**, **16**).

ATCase from *Escherichia coli* is a highly regulated enzyme, comprised of both regulatory and catalytic polypeptide chains. The *Escherichia coli* holoenzyme consists of two identical catalytic homotrimers (100 kDa), and three identical regulatory homodimers (55 kDa) (Figure 3) (**17**). Kinetic studies show that the holoenzyme yields a sigmoidal aspartate saturation curve (**18**). This sigmoidality is amplified or diminished respectively by the nucleotide effectors CTP (inhibitor) and ATP (activator). Isolated catalytic trimers exhibit no regulation, and yield hyperbolic rather than sigmoidal kinetics (**19**).

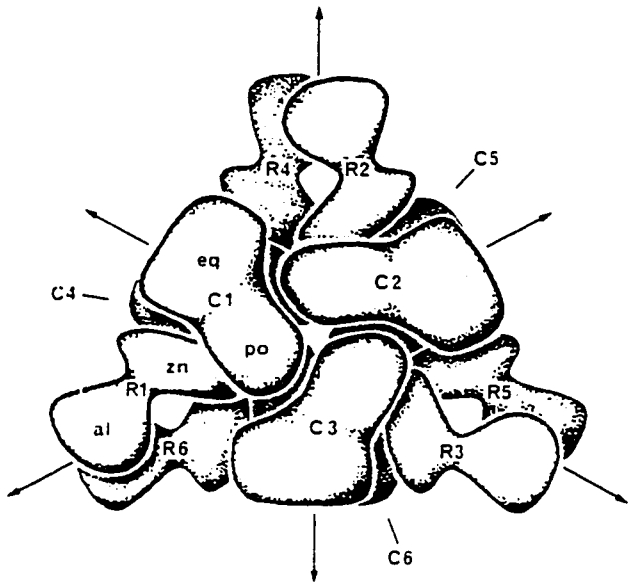

Figure 3: The quaternary structure of aspartate transcarbamylase, viewed down the three-fold axis of symmetry (From Krause, K.L., Volz, K.W., and Lipscomb, W.N. (1985) *Proc. Natl. Acad. Sci. U.S.A.*, **82,** 1643.)

The regulation of ATCase was the initial focus of investigation, and was central in the development of the allosteric model of Monod (**20**) as modified by Kosland (**21**). The kinetic sigmoidality seen in ATCase was attributed by Monod *et al.* to homotrophic allosterism, similar to that seen in the binding of oxygen to hemoglobin (**20**). In this model, the binding of aspartate to a single active site leads to the concerted interconversion of all of the active sites (on a protein molecule), from the (low affinity) T state to the (high affinity) R state. The regulatory effects of the ATP and the CTP were attributed to heterotrophic effects (**20**) that are not seen in the hemoglobin model.

1.2.2 The Kinetic Mechanism of ATCase

The kinetic mechanism that ATCase uses to catalyze its Bi-Bi reaction has remained controversial for 30 years. Initial experiments by Stark and colleagues to determine the kinetic mechanism of ATCase indicated that the catalytic subunits of ATCase use a sequential ordered kinetic mechanism (**22**). Their mechanism proposed that carbamyl phosphate (CbmP) bound first and carbamyl-aspartate was released first (**22**). This conclusion was based on data obtained from isotope exchange studies, partial initial velocity studies, and dead-end product inhibition studies (**22**). Using Cbmp analogues and methods similar to Stark *et al.*, Heyde and Morrison proposed that ATCase catalytic subunits catalyzed a rapid equilibrium random reaction (**23, 24**). Wedler and Gasser then used isotope exchange kinetics to show that the native enzyme catalysed an ordered reaction (**25**). Again using equilibrium isotope exchange experiments, Wedler revised his interpretation of the kinetic mechanism for both the catalytic subunits (**26**) and the holoenzyme (**27**), to that of a preferred ordered random mechanism. To complete the controversy, recent work using heavy atom isotope effects showed that ATCase holoenzyme catalysed a strictly ordered reaction (CbmP binds first, and carbamylaspartate is released first), whereas the reaction catalyzed by isolated catalytic subunits possesses a random component (**28**).

Results in this thesis include the first complete initial velocity plot for catalytic units of ATCase. These results show that this assay is both sensitive and convenient, and can be used to report the Michaelis constants for both substrates in both wild-type ATCase and mutant protein.

1.2.3 The Catalytic Mechanism of ATCase

Although ATCase has been the subject of intense study for many years, only recently has the emphasis of research been upon determining the catalytic mechanism of ATCase. The reaction catalyzed by ATCase is known to be an addition-elimination reaction that proceeds via the formation of a tetrahedral intermediate at the carbonyl carbon of CbmP (**29**) (Figure 4). It is interesting to note that the reaction the enzyme catalyses is unlike the chemical mechanisms for the aqueous decomposition of CbmP i.e. via the formation of a cyanate, and carbamic acid intermediates (**30**).

The mechanism by which the *E. coli* ATCase promotes catalysis remains unclear. There are two ways by which ATCase could promote catalysis: by direct participation in the reaction, or by transition state stabilization. The first case requires the existence of catalytic acids and bases but none have yet been found. For transition state stabilization ATCase would require residues for binding, a conformational flexibility to translocate the substrates to a favorable geometry for the reaction, and possess critical residues to stabilize the transition state of the reaction.

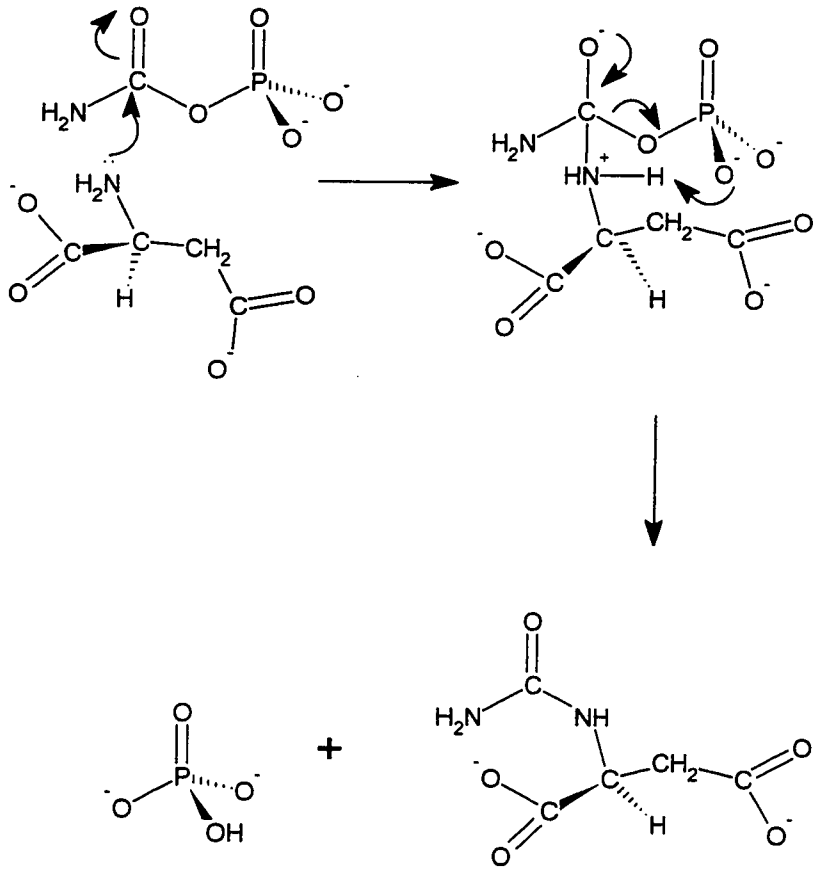

Figure 4: The proposed mechanism for the reaction catalyzed by ATCase: an addition-elimination reaction with the formation of a tetrahedral intermediate at the carbonyl carbon of CbmP.

Figure 5 shows the active site crystal structure of ATCase with the bisubstrate analogue N-(phosphoacetyl)-L-aspartate (PALA). PALA has a nM K_D for ATCase (**31**), is currently being tested as an antiviral agent (**32**), and is in human phase II trials as a chemotherapeutic agent (**33**). Despite its high affinity for the active site, it is unlikely that PALA is a transition state analogue due to the trigonal geometry at the carbonyl carbon of what would be the CbmP moiety. Instead, it is likely that the positioning of the four acidic groups in PALA is ideal for interaction with the substrate binding residues in the active site of ATCase. Further evidence for the bisubstrate nature of PALA is that its nM K_D is similar to the value obtained when multiplying the Michaelis constants for aspartate and CbmP (see Results).

The active site of ATCase is shared between two adjacent catalytic chains (**34**). In the active site, Waldrop *et al.* showed that His134 is involved in orienting the substrates correctly for catalysis (**35**), and that Thr55 is involved in a conformational change prior to catalysis (**36**). However, pH profiles showed that neither residue is involved in acid/base chemistry. Together, Thr55, Arg105, and His134 might work to polarize the carbonyl oxygen of CbmP to facilitate formation of the tetrahedral intermediate. Two residues in *E. coli* ATCase have been published as critical for catalysis, Arg54 (**37**) and Lys84 (**38**). Arg54 is thought to stabilize the phosphate leaving group (**37**), whilst the role of Lys84 remains unexplored.

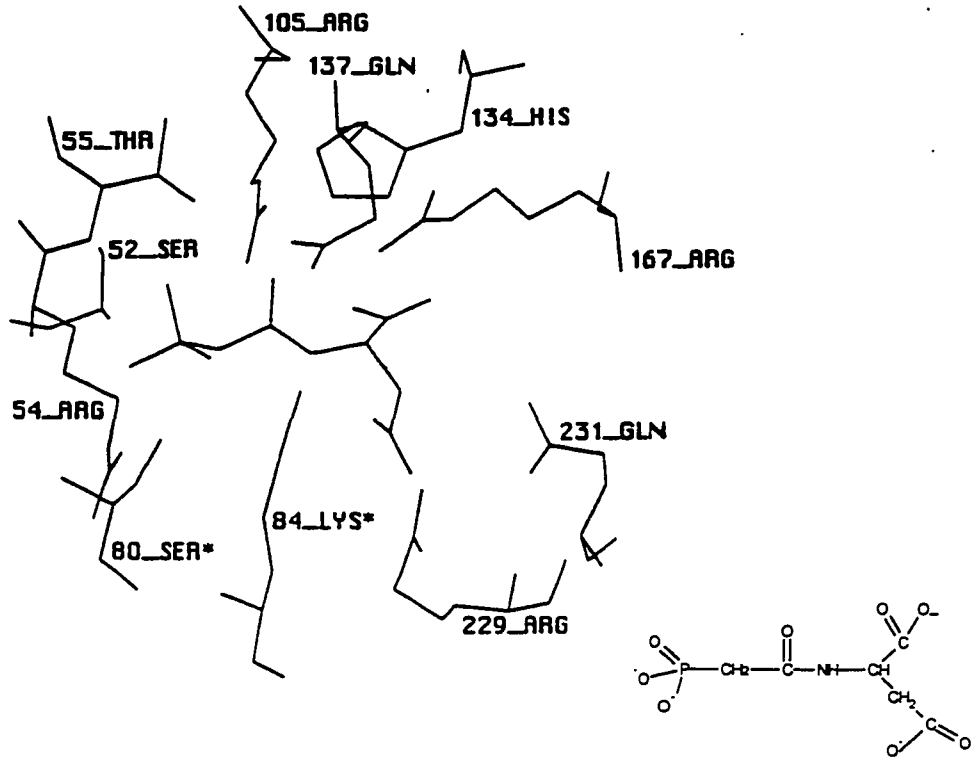

N-(phosphoacetyl)-L-aspartate

Figure 5: The active site of ATCase containing PALA. * Denotes residues contributed by the adjacent catalytic chain (From Waldrop, G.L., Turnbull, J.L., Parmentier, L.E., O'Leary, M.H., Cleland, W.W., & Schachman, H.K. (1992) *Biochemistry* **31,** 6585-6591.)

To summarize the catalytic mechanism: ATCase is a highly regulated enzyme capable of undergoing large conformational changes, with an active site at the interface of two catalytic chains enzyme. ATCase does not appear to capitalize on the chemical lability of CbmP. It has two critical catalytic residues: one with an unassigned role (Lys84), the other stabilizes the phosphate leaving group (Arg54). There are three electrophilic residues near the carbonyl oxygen of CbmP, one of which is involved in a conformational change in order for catalysis to take place. Several substrate binding residues have been identified in the active site (i.e. Arg167, Arg229), but no proton donors or acceptors have been discovered. This evidence suggests a possible role for transition state stabilization in the mechanism of ATCase.

In an attempt to demonstrate the versatility of the m7Ino/PNPase linked assay, this thesis presents the first full pH-rate profile for ATCase using a linked assay. Using a non-linear, interative approach for fitting $1/K_m$ data against pH, this work also reports a new pK value for a group involved with the binding of aspartate to the E-CbmP. To demonstrate the flexibility of the m^7Ino/PNPase-coupled assay, substrate saturation curves for the low activity mutant of ATCase, Lys84 to Gln, will also be presented.

1.3 Introduction to Herpes Simplex Type 1 Helicase-Primase

Herpes Simplex Virus type 1 helicase-primase is an enzyme essential for viral replication (**39**, **40**) and is therefore a primary target for viral inhibition. It is a heterotrimer synthesized from the UL5, UL8, and UL52 genes of the HSV-1 genome (**41**). The HSV-1 helicase-primase holoenzyme exhibits DNA dependant ATPase, helicase, and primase activities.

The UL5 gene contains six motifs exhibited by all members of the superfamily 1 of helicase proteins (**42**). One of these motifs is the "Walker A" motif thought to bind to the di- or triphosphate group of ADP or ATP. Another is the Walker B motif thought to stabilize the co-ordinated magnesium ion (**42**). The UL5 component is thus the likely site for ATP hydrolysis. The UL52 component seems to provide at least part of the primase site as mutations in this subunit can reduce or abolish the primase activity without effecting the helicase activity in the holoenzyme (**43**, **44**).

The core of the enzyme, composed of the UL5 and UL52 products, maintains DNA dependent ATPase and helicase activity (**45**). This subassembly exhibits increasing affinity for, and hydrolysis of, ATP with increasing ssDNA sizes ranging from 12 to 20 nucleotides (**45**). The UL5/52 dimer is, however, inactive in the presence of ssDNA this is coated with the HSV-1 encoded ssDNA binding protein (IPC8). Full activity is restored with the addition of UL8. This suggests a role for the UL8 component as a docking or intermediate protein, acting between the UL5/52 dimer and IPC8 loaded viral DNA (**46**, **47**).

In order to demonstrate that the m7Ino/PNPase linked assay is applicable to a wide range of phosphate liberating enzymes, it is used to assay the DNA dependant ATPase activity of the HSV-1 helicase-primase. An ATP saturation curve will be presented for this low activity, complex, viral protein.

2. MATERIALS AND METHODS

2.1 Materials

Bacterial PNPase (Sigma) was used for initial experiments. However, after completion of cloning, overexpression, and purification of PNPase from *E. coli* (**48**), this product was used as the source of PNPase. Sigma Bacterial PNPase was dissolved in water and stored at -20 °C in 1 mL aliquots (50 U/mL with specific activity of 17 U/mg). A unit of enzyme is defined as the amount of enzyme required to utilize 1 μmol of inosine per minute at 25 °C and pH 7.4.

Cloning, overexpression, and purification of PNPase from *E. coli* was carried out by John Lee. Overexpression was conducted in EK 1104, a strain of *E. coli* lacking the gene for ATCase. This method yielded more than 1000 U of pure PNPase from each liter of culture media (**48**). Pure protein was stored at -20 °C as an ammonium sulfate precipitate. Batches of precipitate were then thawed, resuspended in a minimal amount of water, and dialysed twice against 5 mM MOPS (pH 7.6). This provided PNPase in a form suitable to conduct kinetics, and gave solutions of greater than 700 U/mL PNPase activity. Aliquots of dialyzed enzyme were stored at -20 °C.

m^7Ino was synthesized by the method of Jones & Robins (**49**). The absorption spectra of the product, before and after conversion to m^7Hx by PNPase, were identical to those of commercially available m^7Ino. Its concentration was determined by following the complete phosphorolysis to the product, m^7Hx, λ_{max} = 256 nm (ε = 3.0 x 10^3 $M^{-1}cm^{-1}$ at pH 7.0) (7). Stock solutions of 10 mM m^7Ino in water were prepared on ice and stored at -20 °C in small aliquots. Aliquots were used only once.

Calf thymus DNA was obtained from Boehringer Mannheim and HSV-1 helicase-primase was kindly donated by Bio-Mega/Boehringer Ingleheim Research, Inc. (Quebec).

^{14}C-CbmP (19.6 mCi/mmol) was obtained from Dupont and the unlabelled dilithium salt of CbmP was obtained from ICN. The amount of contaminating free P_i in the commercially available unlabelled CbmP was estimated at 10 % by following the PNPase-catalyzed phosphorolysis of m^7Ino. Without further purification of CbmP, stock solutions were prepared in ice cold water, snap frozen in liquid nitrogen, and stored at -80 °C for later use. All other chemicals were obtained commercially and were of the highest quality available.

Absorbance measurements were taken using a double beam spectrophotometer (GBC Model 918) fitted with thermostatically controlled cuvettes and holders. Cuvettes of 1 mL volume and 1 cm path lengths were used.

Wild-type ATCase was isolated from a strain of *E. coli* TR4363 (his$^-$ pyrF701). This strain contains the multicopy plasmid pPYRB3 (**50**) which carries the intact pyrB-pyrI operon (**51**). The holoenzyme was purified using the procedure of Gerhart and Houlebek with the temperature step omitted (**52**). Catalytic trimers were prepared from the holoenzyme as described by Yang *et al.* (**19**).

Gln84 mutant catalytic subunits of ATCase were obtained from an *E. coli* strain EK 1104 containing the plasmid pPYRB11 with the site specific replacement Lys84 to Gln. This strain was obtained from Ying-Rong Yang, U.C. Berkeley, California. The mutant protein was overproduced by the method of Nowlan and Kantrowitz (**53**), and purified by the same method as for the wild-type enzyme.

2.2 Activity assay for PNPase using m^7Ino.

The specific activity of the *E. coli* overexpressed PNPase was obtained using m^7Ino as a substrate. The spectrophotometric signal of m^7Ino was used to construct a standard curve in order to obtain a value for ΔAbs/μmol phosphate released. When using m^7Ino, rather than Ino, as a substrate the V max for PNPase from *E. coli* is reduced by 14 % (**54**). The spectrophotometric signal of the PNPase activity is then converted into standard units defined for Ino by the following relationship:

U = (ΔAbs/min) / ([ΔAbs/μmol phosphate released] x 0.86)

= μmols Hx converted to Ino / min

2.3 Measurement of ATCase Activity

ATCase activity was determined using the PNPase/m^7Ino coupled assay at 30 °C in a three-component buffer of 50 mM MES, 50 mM MOPS and 100 mM diethanolamine (**55**). The pH of the assay buffer was adjusted using KOH or acetic acid. EDTA (0.2 mM) and the coupling substrate (500 μM m^7Ino) were present in the buffer. When using Sigma Bacterial PNPase, 2 U of the coupling enzyme (PNPase) were added to each assay from stocks of 50 U/mL. When PNPase from *E. coli* was obtained from our laboratory, greater than 15 U were added to each assay from a stock of up to 1000 U/mL.

Unless otherwise indicated, the assays were carried out at pH 8.4 and in 1 mL reaction volumes. Aspartate and CbmP were added at the appropriate concentrations depending on the kinetic constants measured. After the addition of substrates to the buffer, the mixture was incubated for 30 s. This allowed the PNPase/m^7Ino coupling system to remove any P_i present as a contaminant in the CbmP.

The reactions were initiated by the addition of an appropriate amount of ATCase and the reaction rates were recorded as a decrease in Abs_{291} versus time. Initial velocities were determined from the slopes of the progress curves using GBC software. The components of the ATCase assay did not alter PNPase activity.

To monitor the pH-dependence of the kinetic parameters of the ATCase-catalyzed reaction, the amount of Sigma Bacterial PNPase per reaction tube was increased from 2 U (pH 6.4 to 8.4) to 4 U (pH 8.8 and 9.2) and to 6 U (pH 9.6 and 10.0). For Gln84 pH, 10-20 U of *E.coli* PNPase were used. Increasing the amounts of PNPase from these amounts did not increase the rate of m^7Ino phosphorolysis which suggests that the coupling enzyme-catalyzed reaction is not rate-limiting.

The combined rates of CbmP and m^7Ino hydrolysis, determined by monitoring the reaction in the absence of aspartate and ATCase, were subtracted from all enzymatic rates at each pH. Over the time period in which the reaction was followed, the addition of aspartate did not increase these background rates. The concentrations of the holoenzyme and the catalytic trimer of ATCase were determined spectrophotometrically (knowing that 1 mg/mL of each protein gives an Abs_{280} of 0.59 and 0.72, respectively) (**52**). Initial velocities were directly proportional to ATCase concentration over the range used in this study (0.07 - 0.30 μg/mL final concentrations per assay). Reaction velocities are reported in reciprocal seconds and are calculated from the progress curves using the following relationship:

$$V\ (s^{-1}) = (\Delta Abs/min)\ (M_r \text{ active site}) / [(\Delta Abs/\mu mol\ P_i \text{ used})\ (\mu g \text{ enzyme})\ 60\ s]$$

Subunit molecular weights of 33,000 (isolated catalytic trimer) and 50,000 (holoenzyme) were used to calculate turnover numbers per active site.

ATCase activities were also measured at 30 °C using the radioactive stopped-time assay method of Davies *et al.* **(56)** with slight modifications. The buffer system was the same as that used for the continuous spectrophotometric assay. The assay mixtures (0.5 mL total volume) were preincubated for 2 min in a shaking water bath prior to the initiation of the reaction with CbmP. The reaction was terminated by the addition of 0.5 mL of 4 N acetic acid. The reaction tubes were then heated at 100 °C for 20 min. The unreacted radiolabeled CbmP was decomposed with acid and heat and dissipated as $^{14}CO_2$. The labeled product, N-carbamylaspartate, was counted using an LKB 1217 scintillation counter. Under the assay conditions, no more than 15% of the substrate was consumed. Non-enzymatic rates were subtracted from initial velocities.

2.4 Measurement of the DNA-Dependent ATPase Activity of HSV-1 Helicase-Primase

The ATPase activity of helicase-primase was measured at 37 °C in 1 mL reaction mixtures containing 40 mM Hepes (pH 7.5), 10% glycerol, 100 μg calf thymus DNA, 2 mM dithiothreitol, 0 - 5 mM NaATP, 500 μM m^7Ino, and 2 U PNPase. Sufficient $MgCl_2$ was added to maintain the free level of Mg^{2+} at 3 mM, assuming 1 mol of Mg^{2+} complexed per mol of ATP. The reactions were initiated by the addition of 15 μg of HSV-1 helicase-primase and the decrease in absorbance of 291 nm was recorded for 150 s. There was a 5 s lag time before acquiring progress curves. The components of the ATPase assay did not inhibit PNPase activity. This was determined by recording PNPase activity in 40 mM Tris-HCl (pH 7.6) with 500 μM m^7Ino and 3 mM P_i, and comparing values obtained with the addition of the appropriate concentrations of each component of the ATPase assay. The protein concentration of HSV-1 helicase-primase was estimated using the Bio-Rad protein assay kit with bovine serum albumin as a standard. A molecular weight of 287,000 was used to calculate the turnover number per enzyme molecule (**41**).

2.5 Data Analysis

The data were fit to the appropriate equations using the nonlinear regression computer programs of Cleland (**57**) or GraFit (Version 3.0, Leatherbarrow). The values of the parameters obtained from the computer analyses were used to draw the curves in the figures.

Initial velocities (v), obtained by varying the concentration of substrate (A), were substituted into Equation 1 to yield values for the maximum velocity (V), the Michaelis constant for that substrate (K_m), and for the apparent first-order rate constant for the interaction of enzyme and substrate (V/K_m).

Equation 1

$$v = VA / (K_m + A)$$

Kinetic data exhibiting substrate inhibition (at $S = \infty$, $V = 0$) were fit to Equation 2 to obtain values for the maximum velocity (V) and the Michaelis constant for the substrate (K_m) in the absence of inhibition. K_i represents the inhibition constant for the substrate.

Equation 2

$$v = VA / (K_m + A + A^2 / K_i)$$

Kinetic data that exhibited sigmoidal substrate saturation curves were fit to Equation 3 to obtain values for the Hill coefficient (n_H), the substrate concentration at half maximum activity ($S_{0.5}$), and the maximum velocity (V). K' is the effective dissociation constant of the substrate and can be used to solve for $S_{0.5}$ from the relationship $S_{0.5} = K'^{1/n}$

Equation 3

$$v = VA^n / (K' + A^n)$$

Velocity data that gave rise to linear intersecting initial velocity patterns by varying the concentrations of one substrate at fixed concentrations of the other were fitted to Equation 4, where v is the observed velocity, V is the maximum velocity, A and B are the substrate concentrations, K_a and K_b are their respective Michaelis constants, and K_{ia} is the dissociation constants of A from the binary complex.

Equation 4

$$v = VAB / (K_{ia}K_b + K_aB + K_bA + AB)$$

The variation with pH of the values for ΔAbs_{291}, V, and $(V/K_m)_{asp}$ was fit to Equation 5 (full bell intersecting zero). y represents the value of ΔAbs_{291}, V, and $V/K_{m(asp)}$ at a particular pH value. C is the pH-independent maximum of the parameter. K_1 and K_2 are acidic and basic dissociation constants associated with ionizing groups seen in the pH profile.

Equation 5

$$y = C / (1 + [H^+] / K_1 + K_2 / [H^+])$$

The variation with pH of the values for $1/K_{m(asp)}$ was fit to Equation 6 (acidic limb intersecting zero) and Equation 7 (basic limb not intersecting zero). Where y is the $1/K_{m(asp)}$ values, C_1 is the pH independent maximum value of $1/K_{m(asp)}$, and C_2 is the basic minimum value of $1/K_{m(asp)}$. pK1 and pK2 represent the acidic and basic dissociation constants seen in the $1/K_{m(asp)}$ pH profile.

Equation 6

$$y = (C_1 \cdot 10^{(pH - pK1)})/(10^{(pH-pK1)} + 1)$$

Equation 7

$$y= (C_1 + C_2 \cdot 10^{(pH - pK2)})/(10^{(pH -pK2)} + 1)$$

3. RESULTS

3.1 The m^7Ino/PNPase-Coupled Assay

Even though m^7Ino exhibits both fluorescence and absorbance properties, I chose to develop a spectrophotometric assay for phosphate-releasing enzymes, since a spectrophotometer is typically available in most biochemistry laboratories. In order to couple phosphate release to a spectrophotometric signal, the UV spectral shift that accompanies the phosphorolysis of m^7Ino to m^7Hx (Figure 6A) was utilized. The difference spectrum (Figure 6B) demonstrates that m^7Ino exhibits a useful signal ranging from 280 nm to greater than 300 nm, with the maximum signal at 280 nm.

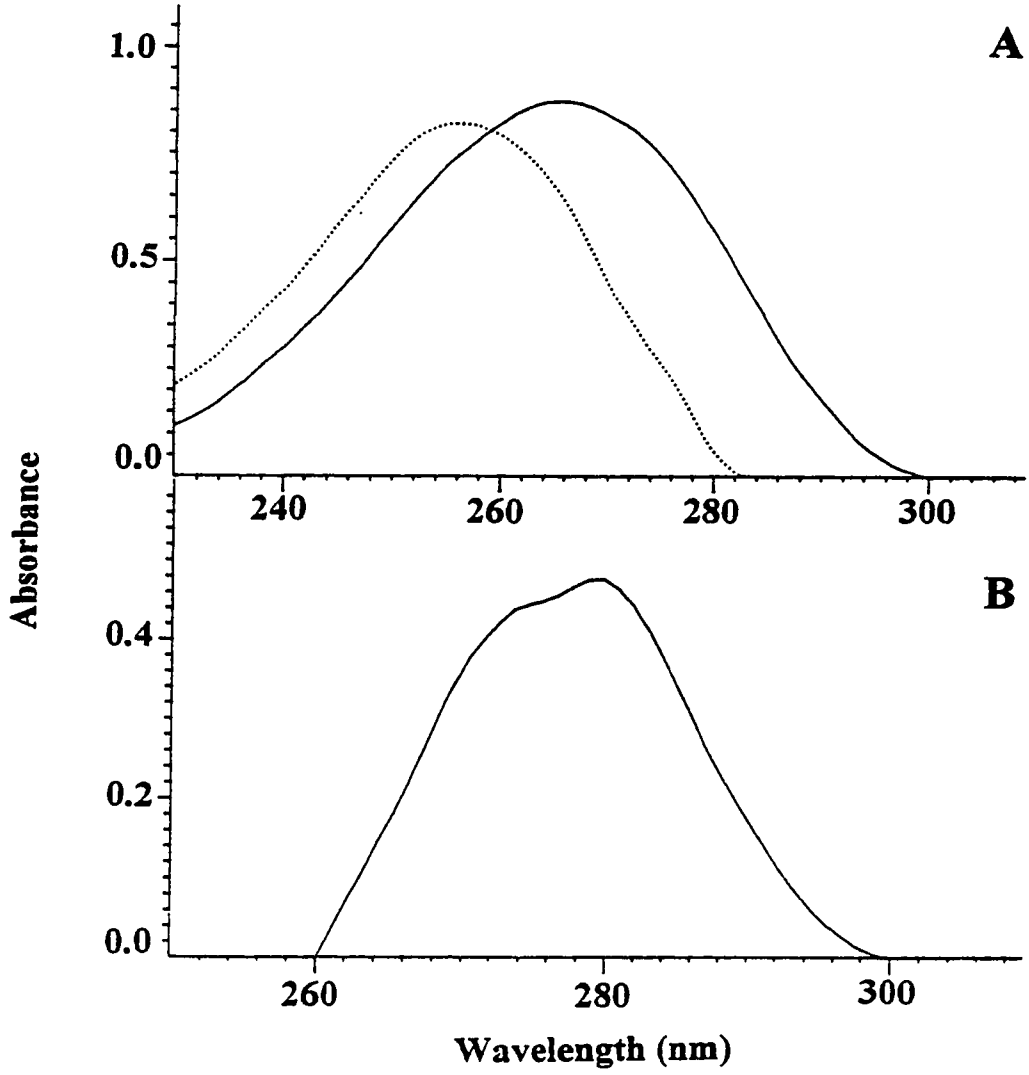

Figure 6: UV spectra in 50 mM MOPS at pH 8.0. (A) m^7Ino (solid line) and m^7Hx (dotted line). (B) Difference spectrum (A-B).

Figure 7 demonstrates the combinations of m^7Ino concentrations and wavelengths used throughout this work. For ATCase initial velocity kinetic plots (Figure 10), the lowest phosphate detection limit was required. To achieve this a combination of 280 nm and 100 μM m^7Ino were used. Figure 7A shows the standard curve, conducted in ATCase buffer (pH 8.4), using this combination of linking substrate and enzyme. Linear regression of the data gives a change of 5.01 Abs units/μmol of m^7Ino converted to m^7Hx (or P_i utilized).

However, 280 nm is in the region of maximal absorbance for protein. Further, the absorbance at 280 nm is too large for coupling substrate concentrations greater than 100 μM and for milimolar concentrations of ATP. Therefore, 500 μM m^7Ino and 291 nm were chosen as values for a general assay of both ATCase and ATPase activity. This combination gave a good spectrophotometric signal (~1 Abs unit for complete phosphorolysis of the 500 μM m^7Ino) and permitted the recording of initial reaction rates using substrates from 50 μM to low millimolar concentrations. Figure 7B shows the phosphate standard curve conducted at 500 μM m^7Ino and 291 nm in the HSV-1 helicase-primase buffer (pH 7.5). Linear regression of this data gives a ΔAbs/μmol of P_i utilized of 2.10.

In order to calculate the specific activity of *E. coli* PNPase, saturating concentrations of m^7Ino were required. This required low sensitivity and was performed by shifting the wavelength to 297 nm in order to observe m^7Ino concentrations of up to 2.5 mM. The phosphate standard curve used to calculate the activity of overexpressed *E. coli* PNPase is shown in Figure 7C. This reduced sensitivity yielded a change of 0.477 Abs units/μmol P_i utilized.

In each case (Figure 7A-C) the data remained linear for more than 95% of the spectrophotometric signal from m^7Ino.

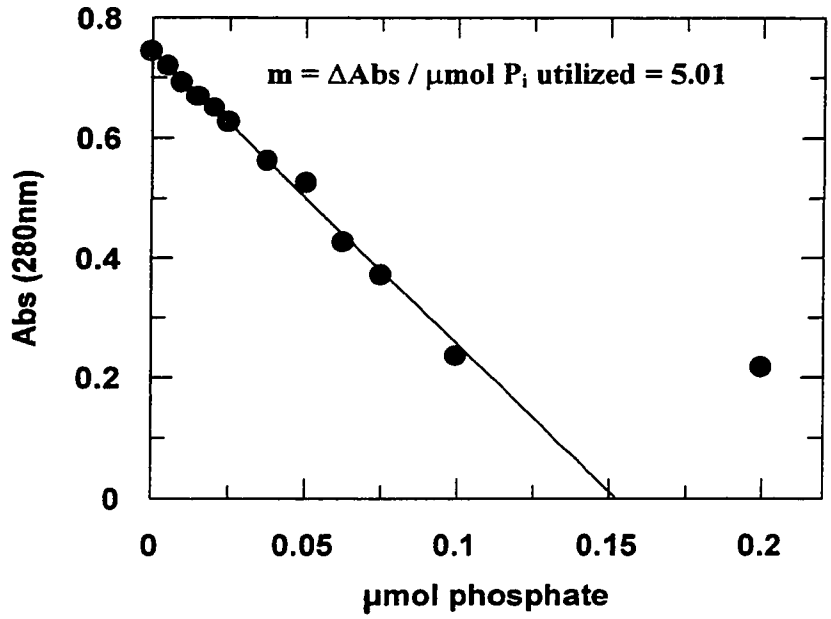

Figure 7A: Changes in absorbance at 280 nm due to the PNPase-catalyzed reaction of m^7Ino as a function of P_i concentration. Reaction mixtures (1 mL) contained ATCase buffer (pH 8.4), 1 U PNPase and 0 - 200 μM KH_2PO_4. Reactions were initiated with 100 μM m^7Ino and after about 10 min, the absorbance at 280 nm was measured. The slope of the linear portion of the curve in (A) gives ΔAbs/μmol P_i used. The line was fitted using linear regression.

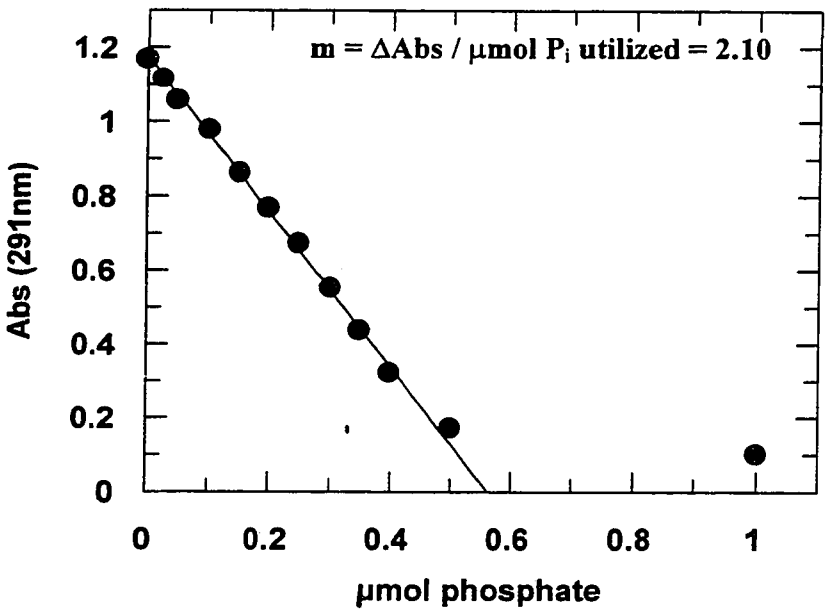

Figure 7B: Changes in absorbance at 291 nm due to the PNPase-catalyzed reaction of m^7Ino as a function of P_i concentration. Reaction mixtures (1 mL) contained HSV-1 helicase primase buffer (pH7.5), 1 U PNPase and 0 - 1 mM KH_2PO_4. Reactions were initiated with 500 μM m^7Ino and after about 10 min, the absorbance at 291 nm was measured.

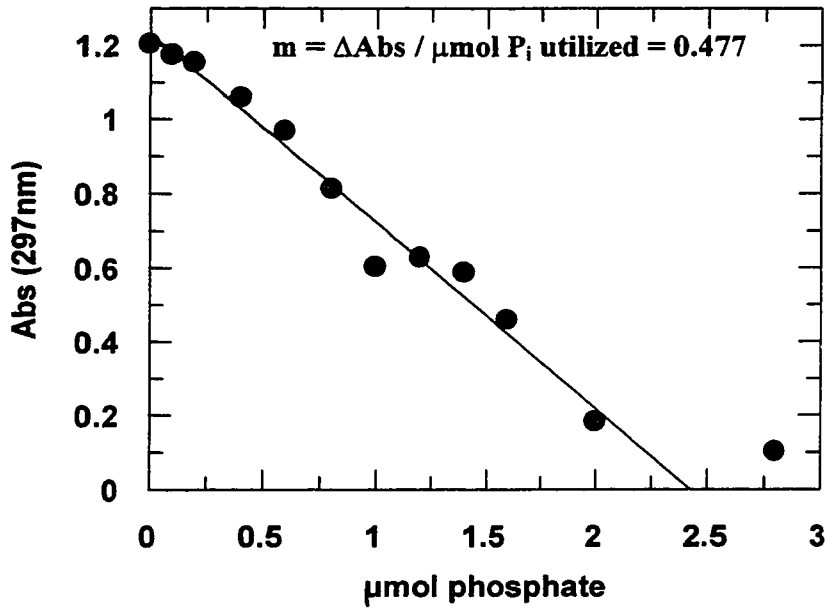

Figure 7C: Changes in absorbance at 297 nm due to the PNPase-catalyzed reaction of m^7Ino as a function of P_i concentration. Reaction mixtures (1 mL) contained 50 mM MOPS (pH 7.5), 1 U PNPase and 0 - 2.8 mM KH_2PO_4. Reactions were initiated with 2 mM m^7Ino, and the absorbance at 297 nm was measured after 10 min.

The effect of pH upon the m^7Ino signal was determined by performing phosphate standard curves in the variable-pH ATCase assay buffer. Figure 8A(i) - (iii) are examples phosphate standard curves conducted at 291nm using 500μM m^7Ino in the ATCase assay buffer at pH 6.4, 8.0, and 10.0. These represent low, middle, and high values in the pH range studied. The data remained linear for more than 95% of the spectrophotometric signal of m^7Ino at pH less than 9, but the signal degenerated as the pH approached pH 10.0 (Figure 8A (iii)).

Figure 8B shows the effect of pH on the spectrophotometric signal seen in Figure 8A. Each point represents the values of ΔAbs/μmol P_i utilized at a particular pH. A bell-shaped curve was obtained. Although the spectrophotometric signal decays at extremes of pH, it is adequate to conduct kinetic measurements in the range of pH 6.0 to pH 10.0. Fitting the data to Equation 5 gives a pH-independent value for ΔAbs/μmol P_i utilized of 2.13 ± 0.03 units; pK values of the signal were estimated at 6.2 ± 0.1 and 9.9 ± 0.1. As the Abs_{291} of m^7Hx varies little at low and medium pH (Figure 8A (i), and (ii)), the pH-dependent changes in absorbances between m^7Ino and m^7Hx are related to effects on m^7Ino. The lower pK corresponds closely to the value of 6.4 for the loss of the zwitterionic form of m^7Ino (**6**). Since the stability of m^7Ino is pH-dependent (**49, 58**), the higher signal pK of 9.9 shown in Figure 8B likely represents the hydrolysis of the strongly absorbing zwitterion of m^7Ino to its product, m^7Hx. Although m^7Hx absorbs poorly at low to neutral pH (see Figure 8A (i), and (ii)), it begins to show significant absorbance at pH > 9 (see Figure 8A (iii)).

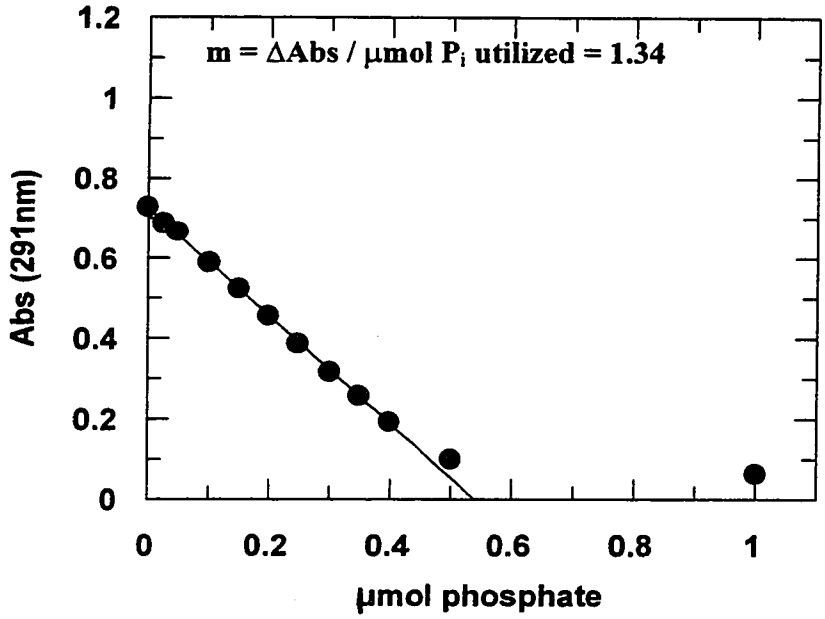

Figure 8A (i): Changes in absorbance at 291 nm (pH 6.4) due to the PNPase-catalyzed reaction of m^7Ino as a function of P_i concentration. Reaction mixtures (1 mL) contained ATCase buffer, 1 U PNPase and 0 - 1 mM KH_2PO_4. Reactions were initiated with 500 μM m^7Ino and after about 10 min the absorbance at 291 nm was measured. The slope of the linear portion of the curve in (A) gives ΔAbs/μmol P_i used. The line was fitted using linear regression.

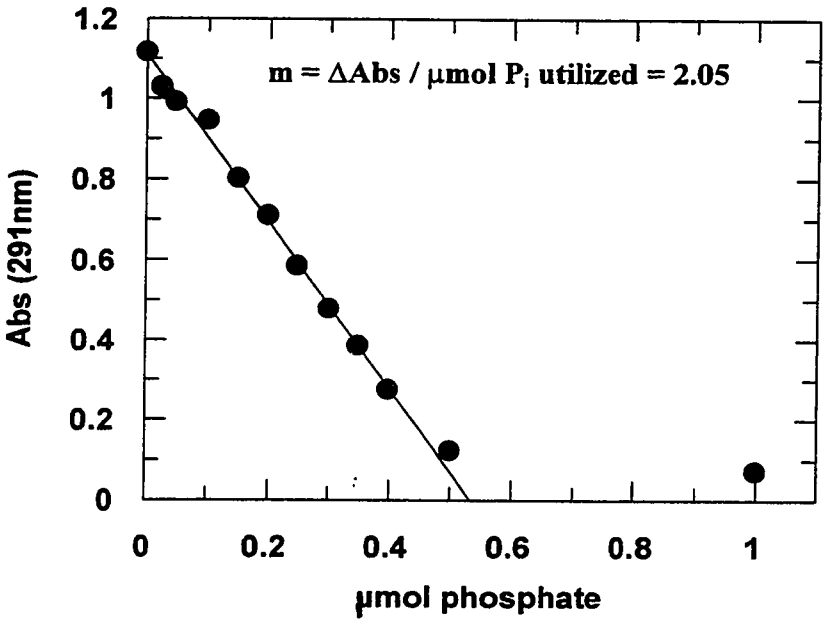

Figure 8A (ii): Phosphate standard curve conducted at pH 8.0 in ATCase assay buffer. Other conditions are as described for Figure 8A (i).

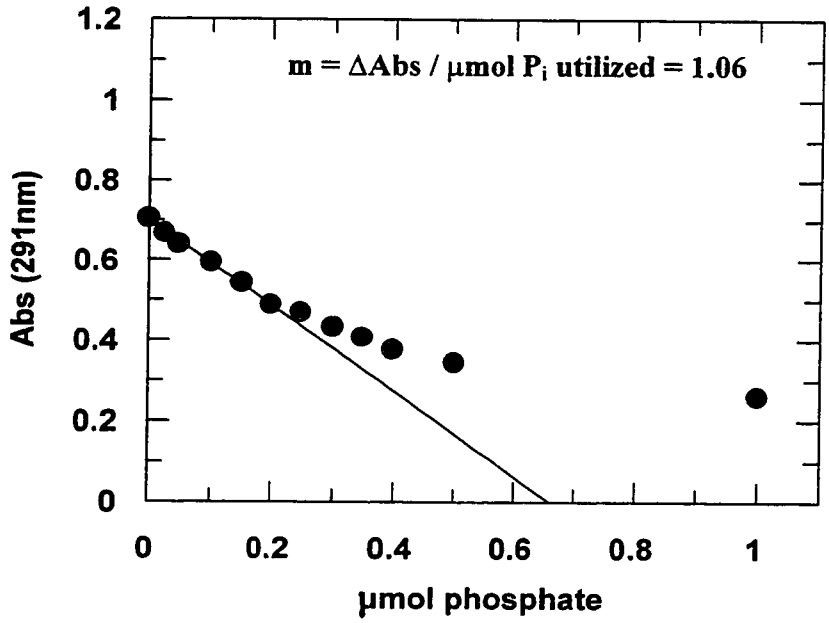

Figure 8A (iii): Phosphate standard curve conducted at pH 10.0 in ATCase assay buffer. Other conditions are as described for Figure 8A (i).

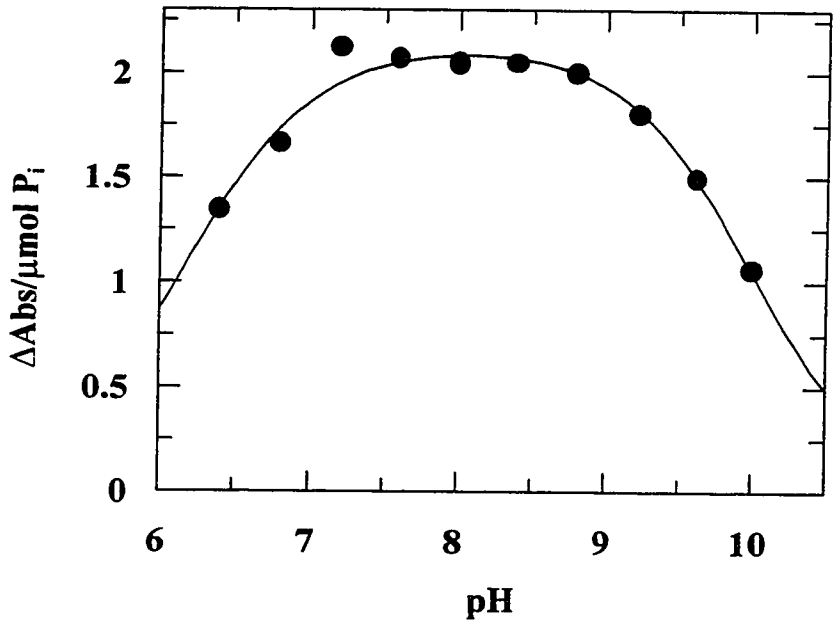

Figure 8B: The effect of pH on the intensity of the UV spectral shift. The pH-dependence of ΔAbs/μmol P_i used represents the best fit of the data to Equation 5.

The PNPase/m^7Ino linked assay proves flexible in many ways. Table 1 summarizes the ΔAbs/μmol P_i values obtained. The first two rows demonstrate that the sensitivity of the assay can be decreased by a factor of ten (from 5.0 to 0.48 Abs units/μmol P_i released) by shifting the wavelength at which the reaction is being monitored, from 280 to 297 nm. Rows 3-5 show that there is very little variation in the signal intensity between pH 7.2 and pH 8.8. In fact, the values obtained at pH 7.2 and pH 8.8 (2.1 and 2.0 respectively) are within 10% of the pH independent value. The final two rows show that both the ATCase and the HSV-1 helicase-primase assay buffers give identical values for ΔAbs/μmol P_i released. As the components of the two sets of buffers differ greatly, this suggests that ionic or other non-specific effects have no effect upon the spectrophotometric signal.

TABLE 1

Values for the PNPase/m^7Ino linked phosphate assay performed under several conditions.

Buffer	[m^7Ino]	Wavelength	pH	ΔAbs/μmol P_i utilized
ATCase[a]	100 μM	280 nm	8.4	5.0
50mM MOPS	2.5 mM	297 nm	7.6	0.48
ATCase	500 μM	291 nm	7.2	2.1
ATCase	500 μM	291 nm	8.8	2.0
ATCase	500 μM	291 nm	pH indep.[c,d]	2.13±0.03
ATCase	500 μM	291 nm	7.6	2.1
HSV-1 helicase-primase[b]	500 μM	291 nm	7.5	2.1

[a] 50 mM MES, 50 mM Mops, and 100 mM Diethanolamine (acetic acid/KOH).

[b]40 mM Hepes (pH 7.5), 10% glycerol, 100 μg calf thymus DNA, 2 mM dithiothreitol, 0 - 5 mM NaATP, and enough $MgCl_2$ to maintain $[Mg^{2+}]_{free}$ at 3 mM.

[c]$pK_1 = 6.2 \pm 0.1$, $pK_2 = 9.9 \pm 0.1$

[d]see Figure 8B.

3.2 Kinetic Characterization of Aspartate Transcarbamylase

3.2.1 Substrate Saturation Curves of ATCase

The substrate saturation curves conducted using the PNPase/m^7Ino continuous assay (500 μM m^7Ino at 291 nm) at pH 8.4 are shown in Figure 9A - C. As expected, data for the isolated catalytic subunits (Figure 9A and B) conform to hyperbolic kinetics while that of the holoenzyme (Figure 9C) yields sigmoidal kinetics. Figure 9A compares aspartate saturation data obtained for the catalytic subunits under assay conditions identical for both the PNPase/m^7Ino coupled approach and the radioactive stopped-time assay. Results for the two different methods are in excellent agreement. Fits of the data from the continuous assay to Equation 1 yields apparent values for K_m (asp) = 4.94 ± 0.36 mM and V = 292 ± 6 s^{-1}, while data from the stopped-time assay gives apparent values for K_m (asp) = 7.49 ± 0.80 mM and V_{app} = 320 ± 12 s^{-1}. Figure 9B shows a saturation curve for CbmP. Fit of the data to Equation 1 give an apparent K_m (CbmP) = 59.5 ± 13.3 μM and V_{app} = 187 ± 9 s^{-1}. These values for the catalytic subunit are, within experimental error, the same as those previously obtained by other methods at pH 8.3 (**59**, **60**, **61**) and the MESG-coupled approach at pH 8.0 (**11**).

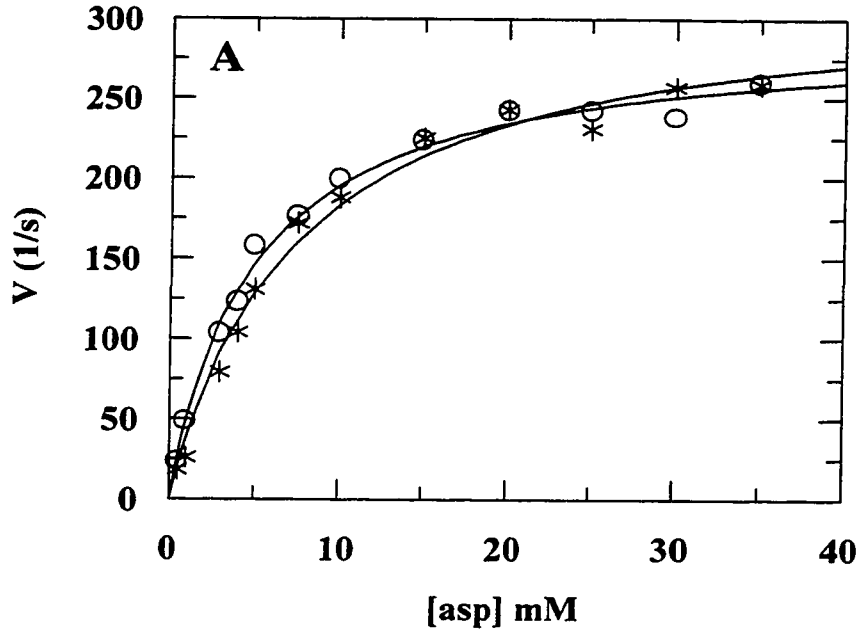

Figure 9A: Aspartate saturation curves for the reaction catalyzed by isolated catalytic subunits of ATCase (pH 8.4). Data were obtained by varying aspartate at a fixed concentration (1 mM) of CbmP using either the PNPase/m^7Ino coupled assay (o--o) or the stopped-time radioactive method (*--*). Velocities for the coupled assay were determined at 291 nm, in the presence of 500 μM m^7Ino, using a value of ΔAbs/μmol P_i released of 2.1 units, and an ATCase concentration of 0.30 μg/mL. The fitted curves represent a best fit of the data to Equation 1.

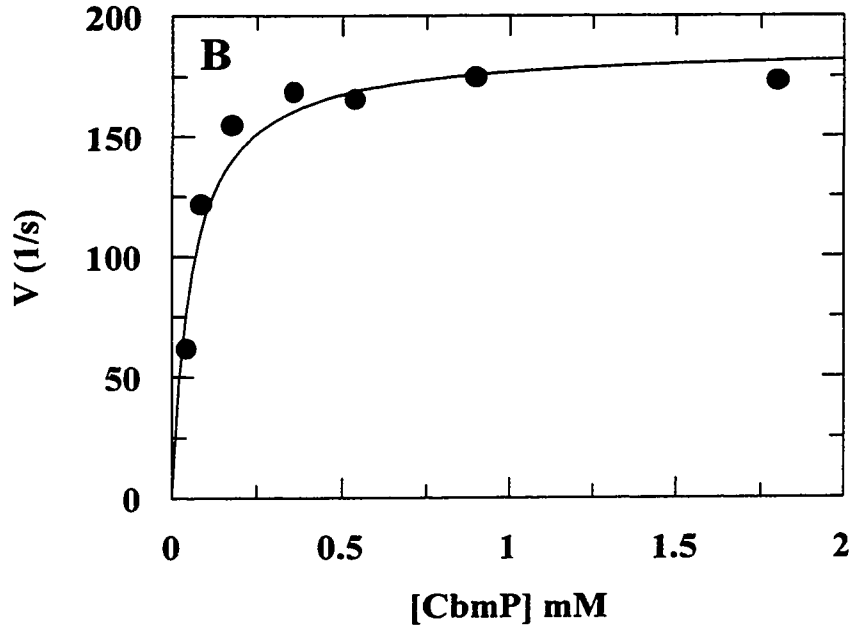

Figure 9B: CbmP saturation curve for the reaction catalyzed by isolated catalytic subunits of ATCase (pH 8.4) using the m^7Ino/PNPase-coupled assay. Data were obtained by varying CbmP concentrations at a fixed concentration (60 mM) of aspartate. Velocities were determined at 291 nm, in the presence of 500 μM m^7Ino, using a value of ΔAbs/μmol P_i released of 2.1 units, and an ATCase concentration of 0.30 μg/mL. The fitted curve represents a best fit of the data to Equation 1.

The saturation curve for aspartate at pH 8.4 and 30 °C for the holoenzyme (Figure 9C (i)) shows clear sigmoidal kinetics. This indicates that this assay can detect positive cooperativity in the binding of aspartate to the holoenzyme. The data were analyzed using Equation 3 to obtain values for V_{app} = 229 ± 11 s^{-1}, $S_{0.5}$ = 10.6 ± 1.8 mM and n_H = 2.6 ± 0.3. The corresponding Hill plot is shown in Figure 9C (ii). The values are within experimental error of those obtained by Wedler *et al.* (**11**) at pH 8.0 using a continuous assay system with PNPase/MESG as the coupling components, as well as by other types of assays at pH 8.0 - 8.3 (**2**, **60**, **62**, **63**, **64**, **65**, **66**). The Hill coefficient was identical when the holoenzyme was assayed by the radioactive stopped-time procedure in the absence or presence of 500 μM m^7Ino. Thus, at this concentration, m^7Ino did not promote or abolish cooperativity in the holoenzyme.

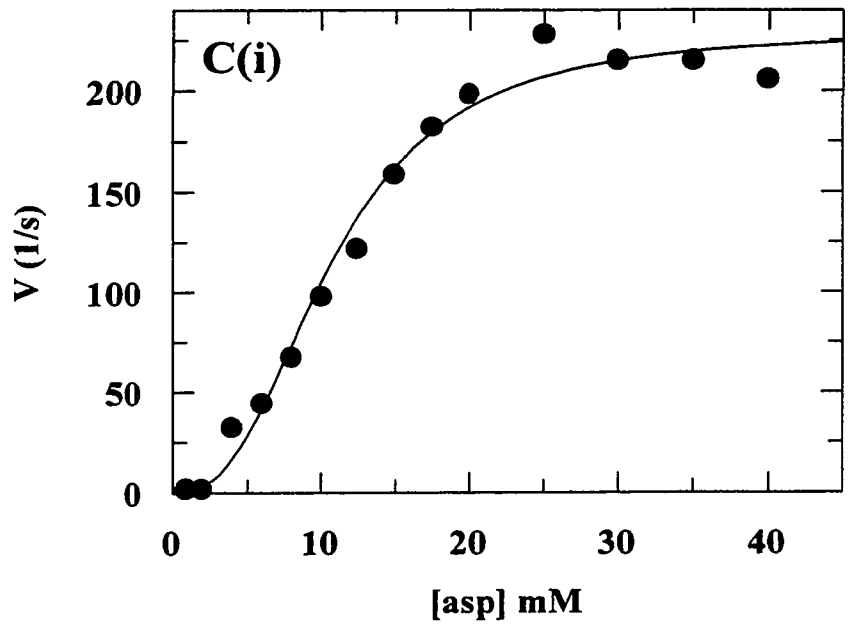

Figure 9C (i): Aspartate saturation curve for the reaction catalyzed by ATCase holoenzyme (pH 8.4). Data were obtained by varying aspartate at a fixed concentration (1 mM) CbmP. Velocities were determined at 291 nm, in the presence of 500 μM m^7Ino, using a value of ΔAbs/μmol P_i released of 2.1 units, and an ATCase concentration of 0.30 μg/mL. The fitted curve represents a best fit of the data to Equation 3.

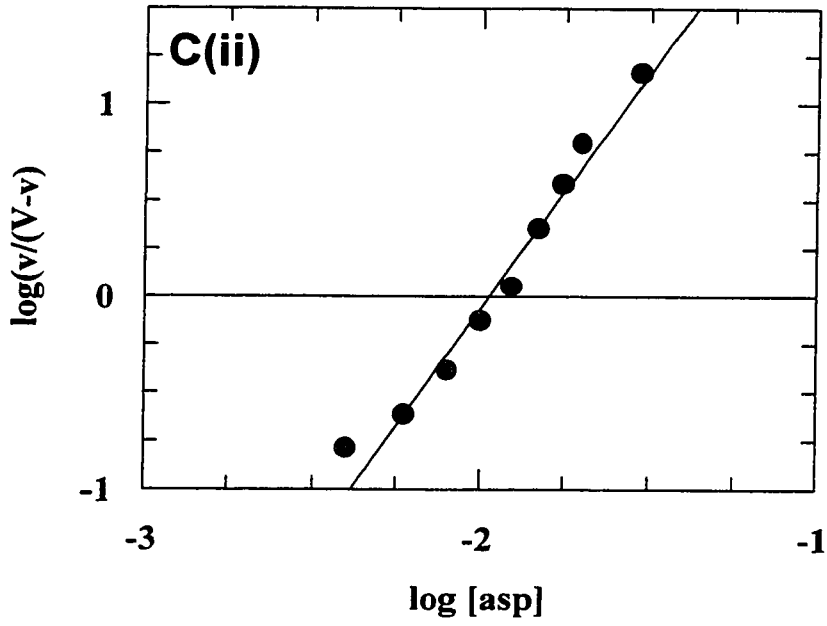

Figure 9C (ii): Hill plot of the aspartate saturation data (Figure 9C (i)) for the reaction catalyzed by ATCase holoenzyme.

3.2.2 Initial Velocity Patterns of ATCase

The sensitivity of the m^7Ino/PNPase-coupled assay to detect ATCase was increased by monitoring the signal at 280 nm using 100 μM m^7Ino. Initial velocity patterns were obtained for the catalytic subunits by varying the concentrations of CbmP (10 - 100 μM) and of aspartate (0.50 - 20 mM). This is the first study of this kind using a continuous assay system. Both plots (Figure 10A and B) are linear and intersect to the left of the y-axis indicating that the reaction conforms to a simple sequential kinetic mechanism. Values for the kinetic parameters obtained by fitting the data to Equation 4 are V = 553 ± 32 s^{-1}, K_a (CbmP) = 36.5 ± 3.9 μM, K_{ia} (CbmP) = 3.51 ± 1.62 μM and K_b (asp) = 6.52 ± 0.66 mM. The value of K_{ia} (CbmP) is within an order of magnitude of those values (7 - 22 μM) obtained by kinetic or equilibrium studies (**24**, **67**, **68**). The value for K_{ib} (asp), which can be derived from the relationship $K_{ib} = (K_{ia})(K_b) / K_a$ (assuming a rapid equilibrium random mechanism), is moderately well-determined at 0.63 ± 0.29 mM.

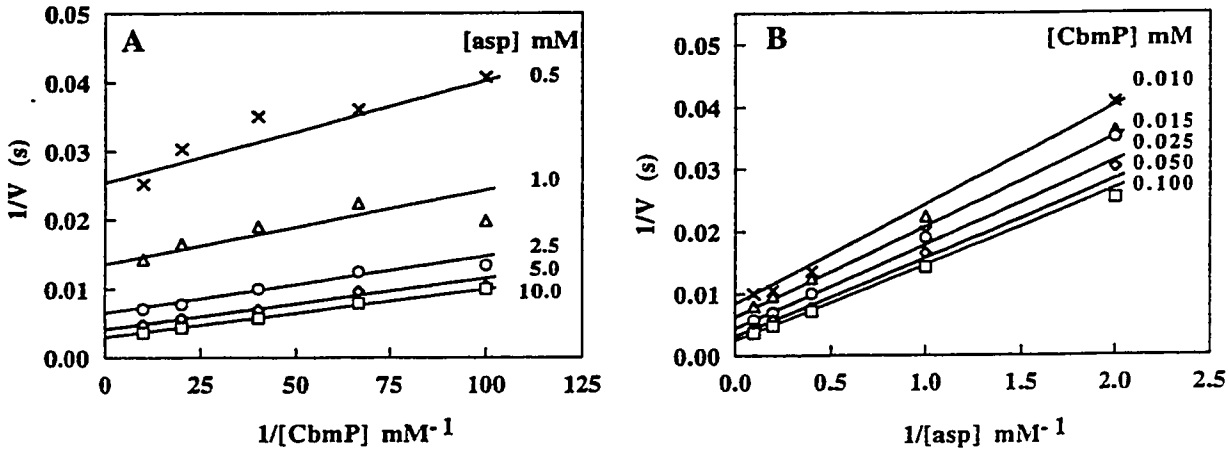

Figure 10: Variation of initial velocity as a function of the concentrations of CbmP (**A**) and aspartate (**B**) for the reaction catalyzed by the catalytic subunits of ATCase at pH 8.4. Velocities were determined at 280 nm, in the presence of 100 μM m^7Ino, using a value of ΔAbs/μmol P_i released of 5.0 units, and an ATCase concentration of 0.07 μg/mL. Curves shown were fitted to Equation 4.

3.2.3 pH-Rate Profiles of ATCase.

The effect of pH on the reaction catalyzed by the catalytic trimers of ATCase was determined over the pH range of 6.4 to 10.0, by varying aspartate concentrations at a concentration of 1 mM CbmP. As seen in Figure 11, log V and log $V/K_{m(asp)}$, and log $1/K_{m(asp)}$ for the wild-type enzyme decrease at both high and low pH values.

Table 2 summarizes the pH sensitive rate constants determined using the m^7Ino/PNPase-coupled assay. Fitting the data for V and $V/K_{m(asp)}$ to Equation 5 yielded pK values of 7.23 ± 0.13 and 10.04 ± 0.17 (V profile), and 6.87 ± 0.18 and 9.27 ± 0.18 ($V/K_{m(asp)}$ profile). The $1/K_{m(asp)}$ acidic limb was fit to a half-bell curve intersecting zero (Equation 6), whilst the basic limb was fit to a half-bell curve not intersecting zero (Equation 7). These fits yielded pK values of 5.85 ± 0.06 for the acidic limb and 8.32 ± 0.08 for the basic limb. The fit of $1/K_m$ to a bell curve intersecting zero was poorer and generated an uneven distribution of errors (**57**), or gave rise to mathematical errors related to the logarithms of a negative number (Grafit). The pK values reported in Table 2 agree with previously published pK values (**67, 69**), with the exceptions being the basic pK of the V profile which has been reported as pK = 9.51 (**67**), and the basic pK of the $1/K_{m(asp)}$ profile which has been reported as pK = 9.0 (**69**). It is interesting to note that the basic pK value for $V/K_{m(asp)}$ of 9.27 is very close to the average of the basic pK values obtained from the V (10.04) and $1/K_{m(asp)}$ (8.32) data (see section 4.2.2).

This thesis presents the first full pH-rate profiles for ATCase conducted using a continuous assay. The close agreement of the wild-type data with previously published work, in conjunction with the linearity of the phosphate standard curve over most of the pH range, suggests that the lability of m^7Ino at alkaline pH (**49**) does not greatly affect initial velocity determinations.

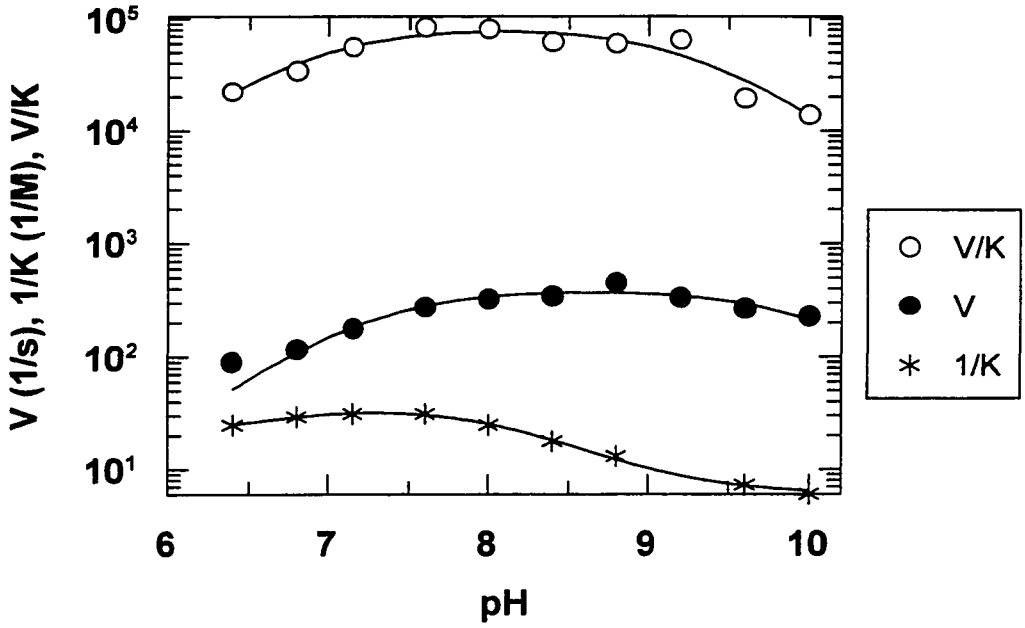

Figure 11: Variation with pH of log V, log $V/K_{m(asp)}$, and log $1/K_{m(asp)}$ for the reaction catalyzed by the wild-type catalytic subunits of ATCase in the presence of1 mM CbmP. Velocities were calculated at each pH by extrapolating values of ΔAbs/μmol P_i released from the curve in Figure 8B. Values for V and $(V/K)_{asp}$ were obtained as described in "Material and Methods" using 0.3 μg of the catalytic subunits. The units for V, $1/K_{m(asp)}$, and $V/K_{m(asp)}$ are s^{-1}, M^{-1}, and $M^{-1}s^{-1}$, respectively. The curves represent the best fits of the data to Equation 5 (V, $V/K_{m(asp)}$), Equation 6, and Equation 7 ($1/K_{m(asp)}$).

TABLE 2

Summary of pH sensitive rate constants for the reaction catalyzed by catalytic subunits of ATCase. Conditions are as reported for Figure 11.

Parameter Determined	Acidic minimum value of parameter	pH independent maximum value of parameter	Basic minimum value of parameter	pK_1	pK_2
V (s^{-1})	0	400 ± 28	0	7.23 ± 0.13	10.04 ± 0.17
$V/K_{m(asp)}$ ($M^{-1}s^{-1}$)	0	$8.6x10^4 \pm 9.6x10^3$	0	6.87 ± 0.18	9.27 ± 0.18
$1/K_{m(asp)}$ (M^{-1}) acidic limb	0	32 ± 0.5	-	5.85 ± 0.06	-
$1/K_{m(asp)}$ (M^{-1}) basic limb	-	34 ± 1.1	5.6 ± 0.9	-	8.33 ± 0.08

3.2.4 Substrate Saturation Curves of Gln84 Catalytic Subunits of ATCase.

The aspartate saturation curve for the Gln84 catalytic subunits of ATCase (Figure 12A) is significantly different from the saturation curves for the wild-type enzyme (Figure 9A). When the data were fit to Equation 1 it yielded apparent values of $V = 0.079 \pm 0.005\ s^{-1}$, and $K_{m(asp)} = 21 \pm 4$ mM. It is striking that the reduction of V by a factor of 4000 occurs with only a three-fold decrease in the enzyme's affinity for aspartate, suggesting that Lys84 is indeed a key catalytic group. CbmP binding is also not significantly affected by this mutation in ATCase. At pH 8.1 Gln84 has a $K_{m(CbmP)} = 400 \pm 130\ \mu M$ (Figure 12B) compared to 60 μM for the wild-type enzyme (Figure 10).

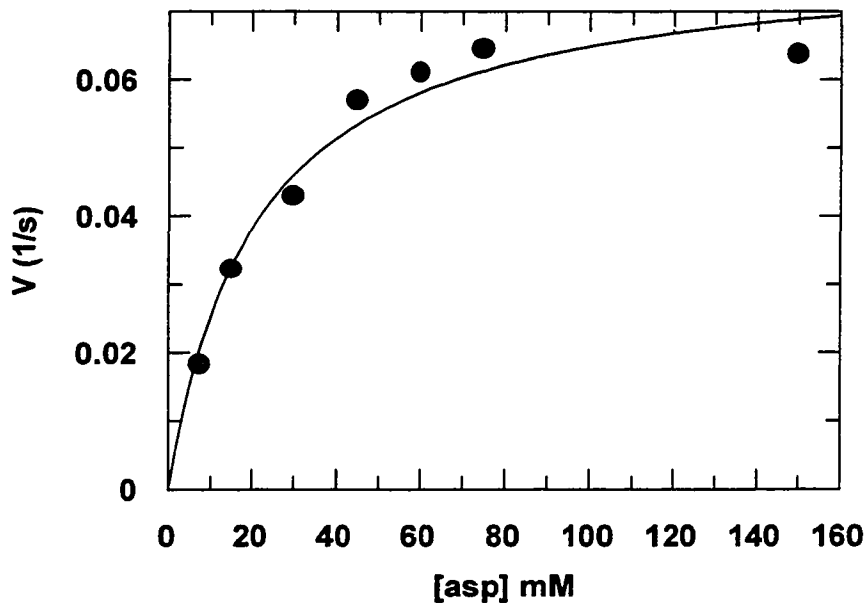

Figure 12A: Aspartate saturation curve for the reaction catalyzed by the isolated catalytic subunits of Gln84 ATCase (pH 8.4). Data were obtained by varying aspartate at a fixed concentration (1 mM) of CbmP. Velocities were determined at 291 nm, in the presence of 500 μM m^7Ino, using a value of ΔAbs/μmol P_i released of 2.1 units, and an ATCase concentration of 250 μg/mL. The fitted curves represent a best fit of the data to Equation 1.

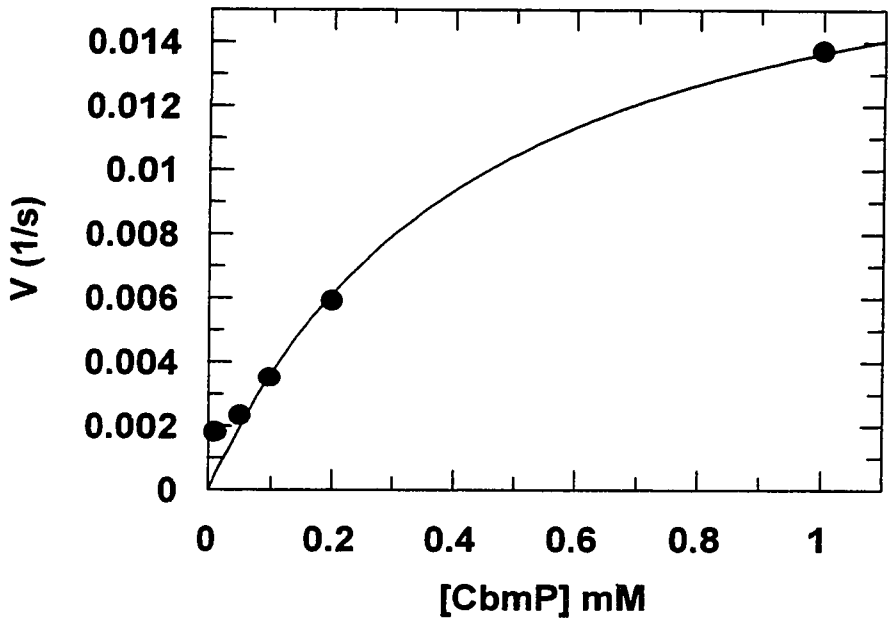

Figure 12B: CbmP saturation curve for the reaction catalyzed by the isolated catalytic subunits of Gln84 ATCase (pH 8.1). Data were obtained by varying aspartate at a fixed concentration (60 mM) of aspartate. Velocities were determined at 291 nm, in the presence of 500 μM m^7Ino, using a value of ΔAbs/μmol P_i released of 2.1 units, and an ATCase concentration of 250 μg/mL. The fitted curves represent a best fit of the data to Equation 1.

3.3 Kinetic Characterization of the DNA-Dependent ATPase of HSV1 Helicase-Primase:

Figure 13 shows the ATP saturation curve for the DNA-dependent ATPase activity of HSV-1 helicase-primase at pH 7.5 and 37 °C. The curve begins to fall-off at high ATP concentrations, characteristic of inhibition by substrate or ionic strength effects. When fit to Equation 2, the data yield well-determined values of $K_{m\,(ATP)} = 0.77 \pm 0.17$ mM and V= $16.5 \pm 2.2\ s^{-1}$. Since the experimental range of ATP concentrations did not exceed 5 mM, the inhibition constant for ATP (K_i) was less reliably-determined at a value of 6.5 ± 2.6 mM. Values for the kinetic parameters $K_{m\ ATP}$ and V compare reasonably well to the previously published values of K_m ATP = 0.61 ± 0.10 mM (**39**) and 1.3 mM (**40**), and V = $35\ s^{-1}$ (**40**), obtained by stopped-time assays with TLC-based or colorimetric detection methods. This is the first report of kinetic constants determined for this ATPase using a continuous spectrophotometric assay.

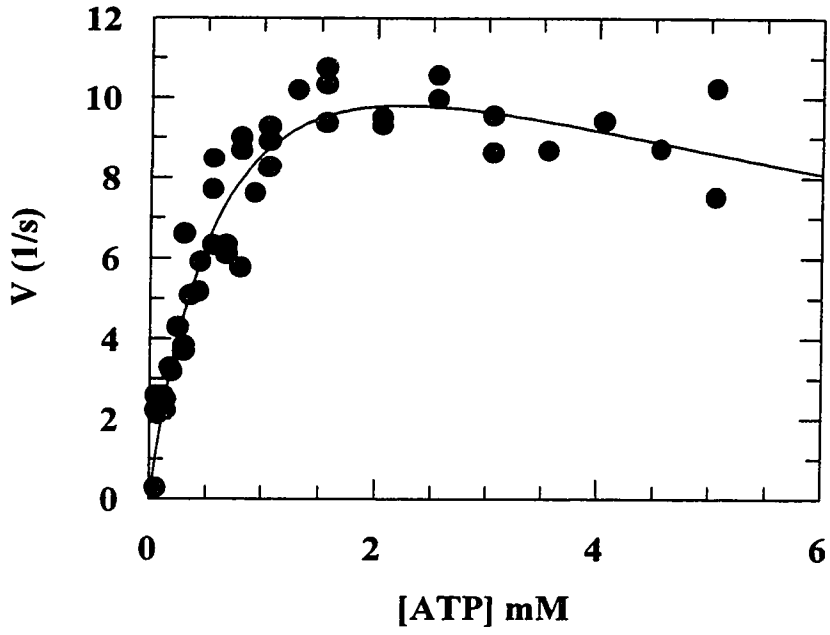

Figure 13: ATP saturation curve for the DNA-dependent ATPase activity of HSV1 helicase-primase at pH 7.5. The ATPase activity was assayed as described in "Material and Methods". Velocities were calculated using a value for ΔAbs/μmol P_i liberated of 2.1 units. The curve represents the best fit of the data to Equation 2.

4. DISCUSSION

4.1 The m^7Ino/PNPase Linked Assay

The findings in this study illustrate that PNPase and m^7Ino, originally used for the quantitation of P_i by fluorimetry (7), can be readily adapted as coupling components for the continuous spectrophotometric assay of phosphate-releasing enzymes such as ATCase and the DNA-dependent ATPase activity of HSV-1 helicase-primase. ATCase catalyzes the carbamylation of aspartate to form N-carbamylaspartate and P_i. Assaying the progress of this reaction has in the past mainly relied on the use of two discontinuous methods that measure the production of N-carbamylaspartate. These include the modified methods (**63**, **70**) of the colorimetric assay of Prescott & Jones (**71**) which involves chemical conversion of N-carbamylaspartate to a chromophoric species, as well as assays using radiolabeled CbmP (**56**) or aspartate (**72**) to detect radiolabeled N-carbamylaspartate. The radioactive methods are sensitive to micromolar concentrations of substrates, but are expensive. In contrast, the relatively insensitive colorimetric assay is widely adopted as a general, inexpensive assay procedure for this enzyme. Both procedures are laborious, particularly the colorimetric assay, which requires overnight incubations in the dark with stringent temperature control. Neither method allows for the convenient determination of initial rates. It is worth noting that ^{14}C-CbmP is no longer commercially available, necessitating the development of this versatile, continuous assay.

Over the past 25 years there have been several continuous assays developed to measure ATCase activity. A titrimetric assay (**73**) uses a pH-stat device to continuously monitor the enzyme-catalyzed proton release. The device is, however, specialized and costly and the analysis can be used only near pH 8.3 where the inorganic phosphate reaction product remains ionized. Foote and colleagues developed two continuous spectrophotometric assays. One assay relied on the fact that the π bond system of N-carbamylaspartate absorbs more strongly at wavelengths between 205 - 215 nm (**74**). Unfortunately its success was linked to the non-UV-absorbing buffer, 1,3 diphosphonopropane (not commercially available), which is somewhat inhibitory of ATCase activity. The second assay (**2**) coupled P_i production with $NADP^+$ reduction using phosphorylase a, phosphoglucomutase and glucose-6-phosphate dehydrogenase (and its various substrates and activators). However, the number of auxiliary enzymes and substrates required make the assay cumbersome, expensive and limited in its application to a narrow pH range, thereby off-setting the attractiveness of its micromolar sensitivity.

More recently, Wedler *et al.* (**11**) adapted a spectrophotometric assay for P_i quantitation (**10**) that had been used for measuring the activities of ATPases (**10**) and protein phosphatases (**12**). This assay was based on the difference in absorbance between a chromophoric nucleoside substrate of PNPase, MESG, and the purine base product of its reaction with P_i. Its high $\Delta\varepsilon$ of 11,000 $M^{-1}cm^{-1}$ at 360 nm and neutral pH makes the signal readily detected in the visible spectrum. Capitalizing on this observation, Wedler *et al.* (**11**) further illustrated the sensitivity of this coupled assay system by constructing substrate saturation curves for both aspartate and CbmP at pH 7 and 8 for the ATCase-

catalyzed reaction. The signal at 360 nm on which this spectrophotometric assay is based is, however, only sensitive from pH 6.5 to about 8.8, corresponding to the maximum UV absorbance difference between MESG (pK 6.5) and it's phosphorolysis product (pK 8.8) (**10**).

The UV spectrophotometric assay method that is outlined here also uses PNPase as the auxiliary enzyme but replaces MESG with m^7Ino as the linking substrate. m^7Ino is a poorer substrate for bacterial PNPase than MESG; the V/K_m ratio for the two nucleoside analogs at pH 7.6 is about 35/1, based on V/K_m values in this study using m^7Ino as a substrate, and those reported using MESG (**10**, **11**). The PNPase/m^7Ino coupling assay I have devised offers several advantages over the method adapted by Wedler *et al.* (11) using MESG. Firstly, m^7Ino is commercially available, and is very easy to synthesize in large quantities from inexpensive starting materials (**49**). Secondly, m^7Ino is very soluble at milimolar quantities whereas MESG is not (**10**). Finally, the change in absorbance at 291 nm between m^7Ino and m^7Hx remains consistently high between pH 7 - 9 and only drops off by one-half at the pH extremes (pH 6.4 and 10) (Figure 8B). In contrast, MESG has lost one-half of its signal at 360 nm by pH 8.8. (**10**). This study represents the first application of a continuous spectrophotometric assay for determining pH profiles for ATCase and it will simplify the kinetic characterization of mutant proteins of ATCase whose pK values are altered (**35**, **36**, **37**, **75**). This assay should be equally amenable to elucidating the chemical mechanisms of other phosphate-releasing enzymes using pH-rate profiles.

The standard assay conditions recording the disappearance of 500 μM m^7Ino at 291 nm and pH 8.4, provided a reasonable spectrophotometric signal (Δ2.1 Abs units/μmol P_i liberated) allowing Michaelis constants for CbmP (micomolar range) and aspartate (milimolar range) to be determined. In order to record accurate initial rates at substrate concentrations 1/10th, their Michaelis constants the sensitivity of the assay was increased 2.5-fold by monitoring the spectrophotometric signal at 280 nm. and by reducing the amount of coupling substrate to 100 μM. Under these conditions, 4 nmol/min P_i can be detected by the m^7Ino/PNPase linked assay. The only other purine nucleoside considered as a substrate for this assay was m^7Guo. Although m^7Guo is a better substrate for bacterial PNPase than m^7Ino by 2.5-fold (**54**), and yields a reasonable absorbance change from its phosphorolysis product m^7Guanine ($\Delta\varepsilon$ = 2,000 M^{-1} cm^{-1}), the window over which any signal occurs is small. Further, the maximum signal is at 260 nm (**54**). The λ_{max} of ATP is also 260 nm, rendering m^7Guo unsuitable in a general phosphate assay for ATPases or for examining the regulation of the holoenyzme of ATCase by ATP and CTP.

A salient point to be addressed when discussing a linked assay is the potential for the introduction of a rate limiting step by the linking components. m^7Ino is a reasonable substrate for *E. coli* PNPase. The apparent K_m for m^7Ino is approximately 250 μM at neutral pH (**54**, **58**), increasing to about 650 μM at pH 8.4 (**58**). The value for V remains relatively constant at about 12 s^{-1} between pH 7.6 and pH 8.4, as does K_m for P_i when using m^7Ino as the nucleoside substrate (200 μM at pH 7.6, and 300 μM at pH 8.4) (**58**). As m^7Ino is a poorer substrate at higher pH, this indicates that the enzyme clearly prefers the cationic form of this nucleoside, while the binding of P_i, and V are essentially pH-

independent (**58**). So while the introduction of a rate-limiting step is not a concern with helicase-primase ATPase, whose turnover number is comparable to that of PNPase at pH 7.5, it is applicable when examining ATCase activities at different pH values.

ATCase has a pH optimum between pH 8 - 9 ($V = 320\ s^{-1}$ at pH 8.4), while PNPase exhibits optimal activity between pH 7 - 8 (**76**). PNPase also has a relatively low affinity for m^7Ino at the pH optimum of ATCase so that at a concentration of 500 μM m^7Ino, PNPase is operating, at best, at about 50% of its maximum velocity. Although this is a concern when using commercial PNPase, the availability of *E. coli* PNPase from our laboratory now makes the cost of adding 10-20 U/assay trivial. While the reaction catalyzed by PNPase is irreversible when using m^7Ino as a substrate, ribose 1-phosphate can act as an end-product inhibitor of the reaction ($K_i = 150$ μM (**54**)). Therefore, care must be taken to follow rates only before product builds up. Finally, studies by Jones and Robins (**49**) show that the stability of m^7Ino is pH-dependent. Hence, initial velocities should be recorded within the first few minutes for assays conducted at pH 10 as m^7Ino decomposes with a half-life of 7 min.

The general nature of this coupled continuous assay has been shown by the kinetic chacterization of ATCase, and another phosphate-releasing enzyme: the DNA-dependent ATPase from HSV-1 helicase-primase. The kinetics of ATCase all lie within experimental error of those reported previously, and are discussed in more detail below. The values obtained in this study for the ATPase are in excellent agreement with those previously reported using both a stopped-time colorimetric assay (**39**) and the radioactive

method with TLC-based detection (**40**). Linear transformation of the data (not shown) support the conclusions of Earnshaw and Jarvest (**39**) that there is a single ATP binding site rather than two sites as suggested by Crute *et al.* (**40**). The reported K_i reflects the drop in enzyme activity at higher concentrations of ATP which has also been noted by Crute *et al.* (**40**). It remains to be determined if this drop in activity is due ionic strength effects or inhibition by ATP.

4.2 Kinetics of Aspartate Transcarbamylase

4.2.1 Initial Velocity Studies of ATCase

Figure 10 shows that ATCase catalytic subunits do not catalyze a rapid equilibrium ordered reaction, since data obtained with aspartate as the variable substrate does not intersect on the y-axis. Figure 10 also rules out ping-pong as a potential kinetic mechanism for ATCase, as the data does not produce a series of parallel lines. Thus, steady-state ordered (**25**, **77**, **22**), rapid equilibrium random (**23**, **24**), and preferred-order random (**26**, **27**) remain as potential candidates for the kinetic mechanism of ATCase. The initial velocity studies presented here represent a marked improvement over the initial velocity study attempted by Heyde *et al.* (**24**). Due to the detection limits of their radioactive stopped-time assay, these authors could only vary CbmP while keeping aspartate at concentrations well below its Michaelis constant. Accordingly, their approach precluded an accurate determination of the Michaelis constant for CbmP and a subsequent value for K_{ib} (asp), using the relationship stated above. Their values of K_{ia} (CbmP) = 7.2 ± 0.9 μM and K_b (asp) = 8.1 ± 0.5 mM were well determined and are in keeping with the results presented here.

These initial velocity plots constitute the first kinetic study on ATCase to provide values for all four kinetic constants simultaneously. The m^7Ino/PNPase assay will thus be useful for further investigation of mutant proteins of ATCase (**35**, **36**, **78**, **79**) which may have an altered kinetic mechanism.

4.2.2 pH-Rate Profiles of ATCase

Table 2 summarizes the pK values obtained by using the m^7Ino/PNPase-coupled assay. Generally these values are close to those previously determined using the radioactive stop-time method for the wild-type enzyme (**67**, **69**). The exceptions are: the basic pK of the V profile (pK = 10.04) which had previously been reported as pK = 9.51 (**67**); and the basic pK for the binding of aspartate to E-CbmP which has been reported as pK = 9.0 using $1/K_{m(asp)}$ data (**69**), and pK = 7.03 to 7.32 derived from K_i profiles for aspartate analogues and the $V/K_{m(asp)}$ profile (**67**). The curves in Figure 11 indicate that two ionizable residues associated with E-CbmP and/or aspartate are involved in the binding of aspartate ($1/K_{m(asp)}$ profile), and that two residues in the ternary complex are essential for catalysis and product release (V profile). In the pH range studied, however, the acidic limb of the $1/K_{m(asp)}$ curve was not well resolved.

The pK values derived from the $V/K_{m(asp)}$ curve represent the protonation state of residues associated with the E-CbmP complex and/or aspartate that are involved in binding and/or catalysis. When fitted to a bell shaped curve, however, the $V/K_{m(asp)}$ data give rise to only two pK values (pK = 6.87 and 9.27). Whereas four unique pK values are obtainable from the separate V (pK = 7.23 and 10.04) and $1/K_{m(asp)}$ data (pK = 5.85 and 8.33). The actual pK values obtained from a $V/K_{m(asp)}$ curve will depend on the shape of the individual V and $1/K_{m(asp)}$ curves, and can represent a mix of the separate V and $1/K_{m(asp)}$ pK values. This apparent loss of information in the $V/K_{m(asp)}$ data is a result of the curve chosen for data fitting. For example, there may well be two basic groups titrating on the basic limb

of the $V/K_{m(asp)}$ profile with pK values of about 8 and 10. However, resolution of these two separate pK values would require many more data points. Thus a determinant in the choice of curves, and the pK values obtained, will be the quality of the data. The V/K profile may not always be the best predictor for the pK values of individual substrate binding or catalytic groups. Care should be taken to always present both V and $1/K_{m(asp)}$ data, when relying on $V/K_{m(asp)}$ data to assign pK values to critical functions.

In ATCase (Figure 11), both the V and the $1/K_{m(asp)}$ curves are concave downward, and the $1/K_{m(asp)}$ curve lies within the concavity of the V curve. At high pH, where all the basic pK values are resolved, the $V/K_{m(asp)}$ (pK = 9.27) is an intermediate value between the pK values derived from the V (pK = 10.04) and $1/K_{m(asp)}$ (pK = 8.33) curves. In ATCase, the fitting of a bell curve intersecting zero to the $V/K_{m(asp)}$ data seems to provide an average of the V and $1/K_{m(asp)}$ pK values.

Turnbull *et al.* (**67**) attributed the basic pK values, obtained when using succinate and cysteine sulfinate, to an aspartate binding group with pK = 7.32. Leger and Herve (**69**) have also reported a pK for the basic limb of the $1/K_{m(asp)}$ as pK = 9. They accomplished this by fitting $1/K_{m(asp)}$ data to a half bell curve intersecting the x-axis (**69**). However, $1/K_{m(asp)}$ data is often a complex relationship of inflections and turning points (**80**). Given that both substrates of ATCase contain at least three ionizable groups, it is likely that a bell shaped curve intersecting zero is not an appropriate curve for 1/K data. For this thesis, attempts at fitting $1/K_{m(asp)}$ data to a half-bell curve intersecting zero led to poor fits and an unequal distribution of errors, or mathematical function errors. This work

suggests that there are two residues (pK = 5.85 and 8.33) important for the binding of aspartate to E-CbmP, titrating in the pH range 6.4 to 10.0. Further studies with substrate analogues will need to be performed in order to determine if these pK values are associated with aspartate or E-CbmP. In general, the pH profiles have proven that the m^7Ino/PNPase assay is a flexible method for conducting complex kinetic studies upon phosphate liberating enzymes.

4.4 Kinetics of Gln 84 Catalytic Subunits of ATCase

These data agrees well with the previous data of Robey *et al.* of V = 0.027 s^{-1}, and $K_{m(asp)}$ = 11 mM (**38**). The comparison of Gln84 and wild-type data shows that this relatively conservative (Lys to Gln) mutation significantly affects catalysis, whilst leaving substrate binding relatively unperturbed. This suggests a key catalytic role for residue Lys84 in the catalytic mechanism of ATCase.

Further characterization of Gln84, using the techniques developed here for the wild-type enzyme, will determine the role of this catalytic residue. The kinetics presented for this mutant protein, together with the HSV-1 helicase-primase data, suggest that the m^7Ino/PNPase-coupled assay is suitable for the investigation of enzymes with very low turnover rates.

5. Conclusions

1. All the constants reported in this work lie within the experimental error of those reported previously. With the synthesis of m^7Ino and the overexpression and purification of PNPase the cost/assay is trivial.

2. The m^7Ino/PNPase spectrophotometric assay has proven reliable for ATCase, an ATPase, and their respective assay conditions. This assay is also flexible in terms of the concentration of m^7Ino used, the signal sensitivity obtained, and types of buffers used. The MESG/PNPase spectrophotometric assay for phosphate is now available in kit form and has been used to assay ATPases, aspartate transcarbamylase, protein phosphatases, and pyrophosphate releasing enzymes. However, the m^7Ino/PNPase-coupled assay has distinct advantages in terms of cost, solubility, and pH flexibility, and will likely supercede the MESG-based assay.

3. This work generated numerous kinetic constants for ATCase. This work provides the first initial velocity plot for ATCase that determines four kinetic constants simultaneously, and shows the first full pH-rate profile for ATCase using a coupled assay. Using this coupled assay I report a new pK value for groups involved the binding of aspartate to E-CbmP, and confirm earlier observations that Lys84 is a critical catalytic group in the active site of ACTase (**38**). This work shows that the m^7Ino/PNPase-coupled assay can, in future, be used to investigate the catalytic and kinetic mechanism of

ATCase. The number of papers (and methods) required to obtain equivalent constants for comparison to this work, demonstrates the overall flexibility of the m^7Ino/PNPase-coupled assay presented here.

6. References

1 Charlot, G. (1966) *Colorimetric Determination of Elements.* Amsterdam: Elsevier Publishing Company, 337-344.

2 Foote, J. and Lipscomb, W. N. (1981) *J. Biol. Chem.* **256**, 11428-11433.

3 De Groot, H., De Groot, H., and Noll, T. (1985) *Biochem. J.* **229**, 255-260.

4 Mushegian, A.R., and Koonin, E.V. (1994) *Protein Science* **3**, 1081-1088.

5 Neuhard, J., and Nygarrd, P. (1987) Purines and Pyrimidines. In: Ingraham,. J.L., Low, K.B., Magasanik, B., Schaechter, M., and Umbarger H.E., eds. *Escherichia coli and Salmomonella typhimurium. Cellular and molecular biology* Washington, D.C.: American Society for Microbiology, 445-473.

6 Krenitsky, T.A., Koszalka, G.W., and Tuttle, J.V. (1981) *Biochemistry,* **20**, 3615-3621.

7 Kulikowska, E., Bzowska, A., Wierzchowski, J., and Shugar, D. (1986) *Biochim. Biophys. Acta* **874**, 355-363.

8 Banik, A., and Roy, S. (1990) *Biochem. J.* **266**, 611-614.

9 Zeng, J., Borchman, D., and Paterson, C.A. (1995) *Curr. Eye Res.,* **14**, 87-93.

10 Webb, M.R. (1992) *Proc. Natl. Acad. Sci.* **89**, 4884-4887.

11 Wedler, F.C., Ley, B.W, and Moyer, M.L. (1994) *Anal. Biochem.* **218**, 449-453.

12 Chen, Q., Wang, Z., and Killilea, S.D. (1995) *Anal. Biochem* **226**, 68-73.

13 Upson, R.H., Haugland, R.P., Malekzadeh, M.N., & Haugland, R.P. (1996) *Anal. Biochem.* **243,** 41-45.

14 Broom, A.D., and Milne, G.H. (1975) *J. Heterocycl. Chem.* **12**, 171-174.

15 Yang, J.L., Fernandes, D.J., Wheeler, K.T., & Capizzi, R.L. (1996) *Int. J. Radiat. Oncol. Biol. Phys.*, **15 34:5,** 1073-1079.

16 Dutta, P.L. & Foye, W.O. (1990) *J. Pharm. Sci.* **79,** 447-450.

17 Krause, K.L., Volz, K.W., and Lipscomb, W.N. (1985) *Proc. Natl, Acad. Sci.U.S.A.* **82,** 1643-1649.

18 Gerhart, J.C., and Pardee, A.B. (1962) *J. Biol. Chem,* **237,** 891-895.

19 Yang,Y.R., Kirschner, M.W., and Schachman, H.K. (1978) *Methods Enzymol.* **51,** 35-41.

20 Monod, J., Wyman, J., and Changeux, J.-P., (1965) *J. Mol. Biol.* **12,** 88-118.

21 Koshland, D.E., Nemethy, G., and Filmer, D. (1966) *Biochemistry* **5,** 365-385.

22 Porter, R.W., Modebe, M.O., and Stark, G.R. (1969) *J. Biol. Chem.* **244,** 1846-1859.

23 Heyde, E., and Morrison, J.F. (1973) *Biochemistry,* **12,** 4718-4726.

24 Heyde, E., Nagabhushanam, A., and Morrison, J.F. (1973) *Biochemistry,* **12,** 4727-4731.

25 Wedler, F.C., and Gasser, F.J. (1974) *Arch. Biochem. Biophys.* **163,** 69-78.

26 Hsuanyu, Y. , and Wedler, F.C. (1988) *Biochim. Biophys. Acta* **957,** 455-458.

27 Hsuanyu, Y. , and Wedler, F.C. (1987) *Arch. Biochem. Biophys.* **259,** 316-330.

28 Parmentier, L.E., O'Leary, M.H., Schachman, H.K., and Cleland, W.W. (1992) *Biochemistry* **31,** 6570-6576.

29 Waldrop, G.L. Urbauer, J.L., & Cleland, W.W. (1992) *J. Am. Chem. Soc.* **114,** 5941-5945.

30 Allen, C.M., & Jones, M.E. (1964) *Biochemistry* **3,** 1238-1247.

31 Laing, N., Chan, W. W.-C., Hutchinson, D.W., & Oberg, B. (1990) *F.E.B.S. Letters* **260,** 206-208.

32 Katsafanas, G.C., Grem, J.L., Blough, H.A. & Moss, B. (1997) *Virology* **236,** 177-187.

33 Wedler, S., Gleissner, B., Hilenfeld, R.U. Thiel, E. Haynes, H. Kaleya, R., Rozenblit, A., & Kreuser, E.D. (1996) *Eur. J. Cancer* **32,** 1254-1256.

34 Wente, S.R., & Schachman, H.K. (1987) *Proc. Natl. Acad. Sci.* **84,** 31-35.

35 Waldrop, G.L., Turnbull, J.L., Parmentier, L.E., O'Leary, M.H., Cleland, W.W., & Schachman, H.K.(1992) *Biochemistry* **31,** 6585-6591.

36 Waldrop, G.L., Turnbull, J.L., Parmentier, L.E., Lee, S., O'Leary, M.H., Cleland, W.W., & Schachman, H.K. (1992) *Biochemistry* **31,** 6592-6597.

37 Stebins, J.W., Robertson, D.E., Roberts, M.F., Stevens, R.C., Lipscomb, W.N., & Kantrowitz, E.R., (1992) *Protein Sci.* **1,** 1435-1446.

38 Robey, E.A., Wente, S.R., Markby, D.W., Flint, A., Yang, Y.R., & Schachman, H.K. (1986) *Proc. Natl. Acad. Sci.* **83,** 5934-5938.

39 Earnshaw, D.L., and Jarvest, R.L. (1994) *Biochem. Biophys. Res. Com.* **199**, 1333-1340.

40 Crute, J.J., Bruckner, R.C., Dodson, M.S., and Lehman, I.R. (1991) *J. Biol. Chem.* **266**, 21252-21256.

41 Crute, J.J., Tsurumi, T., Zhu, L., Weller, S., Olivo, P.D., Challberg, M.D., Mocarski, E.S., and Lehman, I.R. (1989) *Proc. Natl. Acad. Sci. U.S.A.* **86**, 2186-2189.

42 Graves-Woodward, K.L., Gootlieb, J., Challberg, M.D., and Weller, S.K. (1997) *J. Biol. Chem.* **272,** 4623-4630.

43 Klinedinst, D.K. and Challberg, M.D. (1994) *J. Virol.* **68,** 3693-3701.

44 Dracheva, S., Koonin, E.V., and Crute J.J. (1995) *J. Biol. Chem.* **270,** 14148-14153.

45 Healy, S., You, X., and Dodson, M. (1997) *J. Biol. Chem.* **272,** 3411-3415.

46 Tanguy le Gac, N., Villani, G., Hoffmann, J.-S., and Boehmer, P.E. (1996) *J. Biol. Chem.* **271,** 21645-21651.

47 Falkenberg, M., Bushnell, D.A., Elias, P., and Lehman, I.R. (1997) *J. Biol. Chem.* **272,** 22766-22770.

48 Lee, J. (1997) *Overexpression and Purification of Purine Nucleoside Phosphorylase*, Chemistry 450 Honors Thesis, Department of Chemistry and Biochemistry, Montreal: Concordia University.

49 Jones, J.W., and Robins, R.K. (1963) *J. Am. Chem. Soc.* **85,** 193-201.

50 Navre, M., and Schachman, H.K. (1983) *Proc. Natl. Acad. Sci. U.S.A.* **80**, 1207-1211.

51 Pauza, C. D., Karels, M. J., Navre, M., and Schachman, H. K. (1982) *Proc. Natl. Acad. Sci. U.S.A.* **79**, 4020-4024.

52 Gerhart, J. C., and Holoubek, H. (1967) *J. Biol. Chem.* **242**, 2886-2892.

53 Nowlan, S.F., & Kantrowitz, E.R. (1985) *J. Biol. Chem.* **260,** 14712-14716.

54 Bzowska, A., Kulikowska, E., and Shugar, D. (1990) *Z. Naturforsch.* **45c**, 59-70.

55 Ellis, K.J., and Morrison, J.F. (1982) *Methods Enzymol.* **87**, 405-426.

56 Davies, G.E., Vanaman, T.C., and Stark, G.R. (1970) *J. Biol. Chem.* **245**, 1175-1179.

57 Cleland, W.W. (1979) *Methods Enzymol.* **63**, 103-138.

58 Rieger, C.E., Lee, J., & Turnbull, J.L. (1997) *Anal. Biochem.* **246,** 86-95.

59 Stebbins, J.W., Xu, W., and Kantrowitz, E.R. (1989) *Biochemistry* **28**, 2592-2600.

60 Middleton, S.A., and Kantrowitz, E.R. (1988) *Biochemistry* **27**, 8653-8660.

61 Xu, W., and Kantrowitz, E.R. (1991) *Biochemistry* **30**, 2535-2542.

62 Stevens, R.C., Chook, Y.M., Cho, C.Y., Lipscomb, W.N., and Kantrowitz, E.R. (1991) *Protein Eng.* **4**, 391-408.

63 Else, A.J., and Herve, G. (1990) *Anal. Biochem.* **186**, 219-221.

64 Strange, C.J., Wales, M.E., Brown, D.M., and Wild, J.R. (1993) *Biochemistry* **32**, 4156- 4167.

65 Baker, D.P, and Kantrowitz, E.R. (1993) *Biochemistry* **32**, 10150-10158.

66 Xi, G.X., De Staercke, C., Van Vliet, F., Triniolles, F., Jacobs, A., Stas, P.P., Ladjimi, M.M., Simon, V., Cunin, R., and Herve, G. (1994) *J. Mol. Biol.* **242**, 139-149.

67 Turnbull, J.L., Waldrop, G.L., and Schachman, H.K. (1992) *Biochemistry* **31**, 6562-6569.

68 Suter, P., and Rosenbusch, J.P. (1976) *J. Biol. Chem.* **251**, 5986-5991.

69 Leger, D., and Herve, G. (1988) *Biochemistry* **27**, 4293-4298.

70 Pastra-Landis, S.C., Foote, J., and Kantrowitz, E.R. (1981) *Anal. Biochem.* **118**, 358-363.

71 Prescott, L.M., and Jones, M.E. (1969) *Anal. Biochem.* **32**, 408-419.

72 Porter, P.W., Modebe, M.O., and Stark, G.R. (1969) *J. Biol. Chem.* **244**, 1846-1859.

73 Wu, C-W., and Hammes, G. (1973) *Biochemistry* **12**, 1400-1408.

74 Foote, J. (1983) *Anal. Biochem.* **134**, 489-494.

75 Yuan, X.L., Licata, V.J. and Allewell, N.M. (1996) *J. Biol. Chem.* **271**, 1285-1294.

76 Jensen, K.F., and Nygaard, P. (1975) *Eur. J. Biochem.* **51**, 253-265.

77 Schaffer, M.H., and Stark, G.R. (1972) *Biochem. Biophys. Res. Comm.* **46**, 2082-2086.

78 Wedler, F.C., Ley, B.W., Lee, B.H., O'Leary, M.H. and Kantrowitz, E.R. (1995) *J. Biol. Chem.* **270**, 9725-9733.

79 Hsuanyu, Y., Wedler, F.C., Kantrowitz, E.R. and Middleton, S.A. (1989) *J. Biol. Chem.* **264**, 17259-17265.

80 Kyte, J. (1995) *Mechanism in Protein Chemistry.* New York N.Y.: Garland Publishing Inc. p.272.